EXAMINATION OF SELECTED PASSIVE TRACKING SCHEMES USING ADAPTIVE KALMAN FILTERING

by

Timothy E. Dailey

Thesis submitted to the Faculty of the

Virginia Polytechnic Institute and State University

in partial fulfillment of the requirements for the degree of

MASTER OF SCIENCE

in

Electrical Engineering

APPROVED:

R. L. Moose, Chairman

I. M. Besieris

R. Lumia

June, 1982

Blacksburg, Virginia

ACKNOWLEDGMENTS

I would like to thank my advisor Dr. R. L. Moose for providing me with the opportunity to conduct the research discussed herein. His support and encouragement were invaluable during the course of this research.

I would also like to thank my committee members, R. Lumia and I. M. Besieris, for their careful reading and consideration of this thesis.

TABLE OF CONTENTS

page

1. INTRODUCTION AND DISCUSSION OF BACKGROUND MATERIAL 1

   1.1 Introduction 1

   1.2 Overview of Target Tracking 2

   1.3 Development of the Target Model 4

2. DEVELOPMENT OF A SIMPLE RANGE ESTIMATOR USING TIME-DELAY MEASUREMENTS 11

   2.1 Overview 11

   2.2 Discussion of Time-Delay Measurements 11

   2.3 Discussion of the Linearizing Prefilter 13

   2.4 Results From a Matched Kalman Filter Range Tracker 18

3. DEVELOPMENT OF AN ADAPTIVE RANGE TRACKER 23

   3.1 Introduction to the Adaptive Filtering Approach 23

   3.2 Performance Analysis of the Adaptive Range Tracker . . . 28

   3.3 Conclusion 35

4. INTRODUCTION TO PASSIVE TRACKING USING FREQUENCY MEASUREMENTS 37

   4.1 Introduction 37

   4.2 Fundamental Doppler Principles 37

   4.3 Velocity Tracking Using the Doppler Effect with Known Constant Center Frequency 39

   4.4 Conclusions 45

5. PASSIVE TRACKING USING THE DOPPLER EFFECT WITH A RANDOM CENTER FREQUENCY 47

   5.1 Introduction 47

   5.2 Development of a Random Center Frequency Estimation . . . 47

TABLE OF CONTENTS (Continued)

page

5.3 Performance of the Velocity Tracker With Random Center Frequency 52

5.4 Conclusion 58

6. CONCLUDING REMARKS 59

REFERENCES 61

APPENDIX A 62

1. INTRODUCTION AND DISCUSSION OF BACKGROUND MATERIAL

1.1 Introduction

During the past several decades, a great deal of energy has been expended in the development of tracking systems for maneuvering targets. Though many workable systems have been developed, tracking problems continue to command a great deal of research effort, for a "best" tracking solution has not yet been found. There is always a more accurate, faster, or simpler approach waiting to be discovered.

This situation is particularly true in the field of SONAR where the ocean environment and its inefficiencies as an acoustical wave guide provide tremendous obstacles to target tracking. The complexities introduced by the ocean medium necessitate novel problem approaches and constant reevaluation of current tracking systems from different perspectives in order to advance the state of the art. One current tracking system has been proposed by Moose and McCabe [1]. Their approach provides good results in its present form; however, close examination of their method reveals the possibility for slightly different approaches which could lead to better results.

In this thesis, we shall explore the feasibility of several new approaches to passive SONAR tracking developed from Moose and McCabe's work. No attempt will be made to develop "polished" tracking systems. The goal here is simply to provide results which confirm the validity of the approach and inspire further development toward a "polished" final tracking system.

1.2 Overview of Target Tracking

Most of the research done in the target tracking field has centered on the development of target models and associated digital filtering algorithms. One common approach has been to model target dynamics in rectangular coordinates and then use an associated extended Kalman filter (EKF) to process measurement data. The rectangular coordinate system produces linear state equations, but the measurements are nonlinear functions of the state variables. These measurement nonlinearities necessitate an EKF. Unfortunately, EKF's have been found to provide poor estimates or even diverge under adverse conditions such as an abrupt target maneuver. To avoid the nonlinearities of rectangular coordinates, Moose and Gholson developed a target model using polar coordinates [1].

Besides the coordinate system, the method of modeling target maneuvers must also be considered. A logical progression of modeling improvements has led to a very useful and realistic target model [2]. This model considers a typical target trajectory to be the response of a time-correlated random acceleration [3] while large scale trajectory changes are modeled by a semi-Markov process [1] and [4]. More specifically, the target model forcing function is viewed as a correlated random process whose mean value randomly switches between a finite-preselected set of values. The correlated random process, developed by Singer [3], models target velocity changes which are beyond the target's control, such as ocean current changes and random fluctuations in engine output. Deliberate target maneuvers are

modeled as a semi-Markov process and account for the randomly switching mean. Each "state" of the Markov process represents a specific target velocity. The amount of time a target remains in the same state, or equivalently at the same velocity, is considered random; therefore, requiring a semi-Markov model.

In earlier versions of this model [2], many Markov "states" were required to adequately approximate the velocity continuum available to a real target, which in turn, allowed proper convergence of the estimation filters. However, it has been shown in [5] that the current target model requires only a small number of states to assure proper filter convergence.

The above target model was successfully incorporated into a Bayesian estimator by Moose [4]. This tracking system adaptively weights a bank of Kalman filters, each conditioned on a preselected target state or velocity, to produce an estimate of the actual target state. This adaptive scheme and its associated polar target model are fundamental to this text and will be discussed more fully in due course.

The adaptive approach is not the only solution available to the maneuvering target tracking problem. Other techniques have been proposed by Jazwinski [6] who artificially maintains filter gains at a level which will allow detection of a maneuver. Thorp [7] has developed a tracking system which switches between two Kalman filters in response to a detected maneuver.

1.3 Development of the Target Model

The following equations form the basis for the development of the target dynamics model discussed in the previous section.

$$\ddot{x} + \alpha\dot{x} = U_x + w'_x \tag{1.3.1}$$

$$w'_x + aw'_x = w(t) \tag{1.3.2}$$

where

$w(t)$ is a Gaussian white noise process

a is the Singer correlation time constant

α is a drag coefficient

x is any rectangular coordinate

U_x is the time varying mean value of $w(t)$ which controls the target's velocity and maneuvers.

The first equation describes the acceleration of a target in any one dimension of a rectangular coordinate system. This acceleration is driven by a Singer correlated process w'_x which is described by equation 1.3.2.

As we mentioned in the previous section, U_x describes the target's chosen velocity and the correlated Gaussian noise process accounts for random fluctuations which are beyond the target's control. The relationship between U_x and the target's velocity is fundamental to an understanding of subsequent material and shall, therefore, be examined at this time. Under steady state conditions, $\ddot{x}$ in equation 1.3.1 is zero and on the average w'_x is also zero. So, on the average,

the steady state version of 1.3.1 is

$$\alpha\bar{\dot{x}} = U_x \tag{1.3.3}$$

Now solving for $\bar{\dot{x}}$, the average velocity, we have

$$\bar{\dot{x}} = \frac{U_x}{\alpha} \tag{1.3.4}$$

The average velocity is actually the target's chosen velocity before it is corrupted by random fluctuations. So, the target's chosen velocity is simply related to U_x by the reciprical of α. Because of this simple relationship, the reader should think of U_x and U_s, to be defined later, as velocity terms in subsequent discussions.

The final target model is derived by enlisting two sets of equations 1.3.1 and 1.3.2 to describe a target's motion in the x and y directions where the x-y plane is considered parallel and fixed with respect to the ocean floor. After placing the x and y coordinate equations in state variable form, the final polar model is reached through a truncated Taylor series expansion of the nonlinear transformation from rectangular to polar coordinates. An outline of the complete target model derivation [1] is given below.

By selecting x, $\dot{x}$, and w'_x as the state variables, 1.3.1 and 1.3.2 can be placed in the following discrete state variable form:

$$\underline{X}(k+1) = \phi\, \underline{X}(k) + \Gamma\, \underline{U}(k) + \psi\, w(k)$$

or

$$\begin{bmatrix} x \\ \dot{x} \\ w'_x \end{bmatrix}_{k+1} = \begin{bmatrix} 1 & A & B \\ 0 & E & F \\ 0 & 0 & e^{-aT} \end{bmatrix} \begin{bmatrix} x \\ \dot{x} \\ w'_x \end{bmatrix}_{k} + \begin{bmatrix} C \\ A \\ 0 \end{bmatrix} U_x(k) + \begin{bmatrix} D \\ G \\ J \end{bmatrix} w(k) \quad (1.3.5)$$

where T is the sample time and

$$A = (1 - e^{-\alpha T})/\alpha$$

$$B = [1 + (ae^{-\alpha T} - \alpha e^{-aT})/(\alpha - a)]/(\alpha a)$$

$$C = (\alpha T - 1 + e^{-\alpha T})/\alpha^2$$

$$D = [T + (aA - \alpha J)/(\alpha - a)]/(\alpha a)$$

$$E = e^{-\alpha T}$$

$$F = (e^{-aT} - e^{-\alpha T})/(\alpha - a)$$

$$G = (J - A)/(\alpha - a)$$

$$J = (1 - e^{-aT})/a$$

k is the discrete time parameter

Note that equation 1.3.5 describes target motion only in the x direction. A similar set of state equations can be derived for the y direction.

We now wish to combine the state variable expression for the x and y coordinate into a polar form which models range, ρ, and range rate, $\dot{\rho}$. This is done by expanding equation 1.3.6 in a Taylor series keeping only the linear terms.

$$\rho = [(x_s - x_o)^2 + (z_s - y_o)^2]^{1/2} \quad (1.3.6)$$

Figure 1.3.1 and Table 1.3.1 should serve as an explanation of the geometry and terms used in this development.

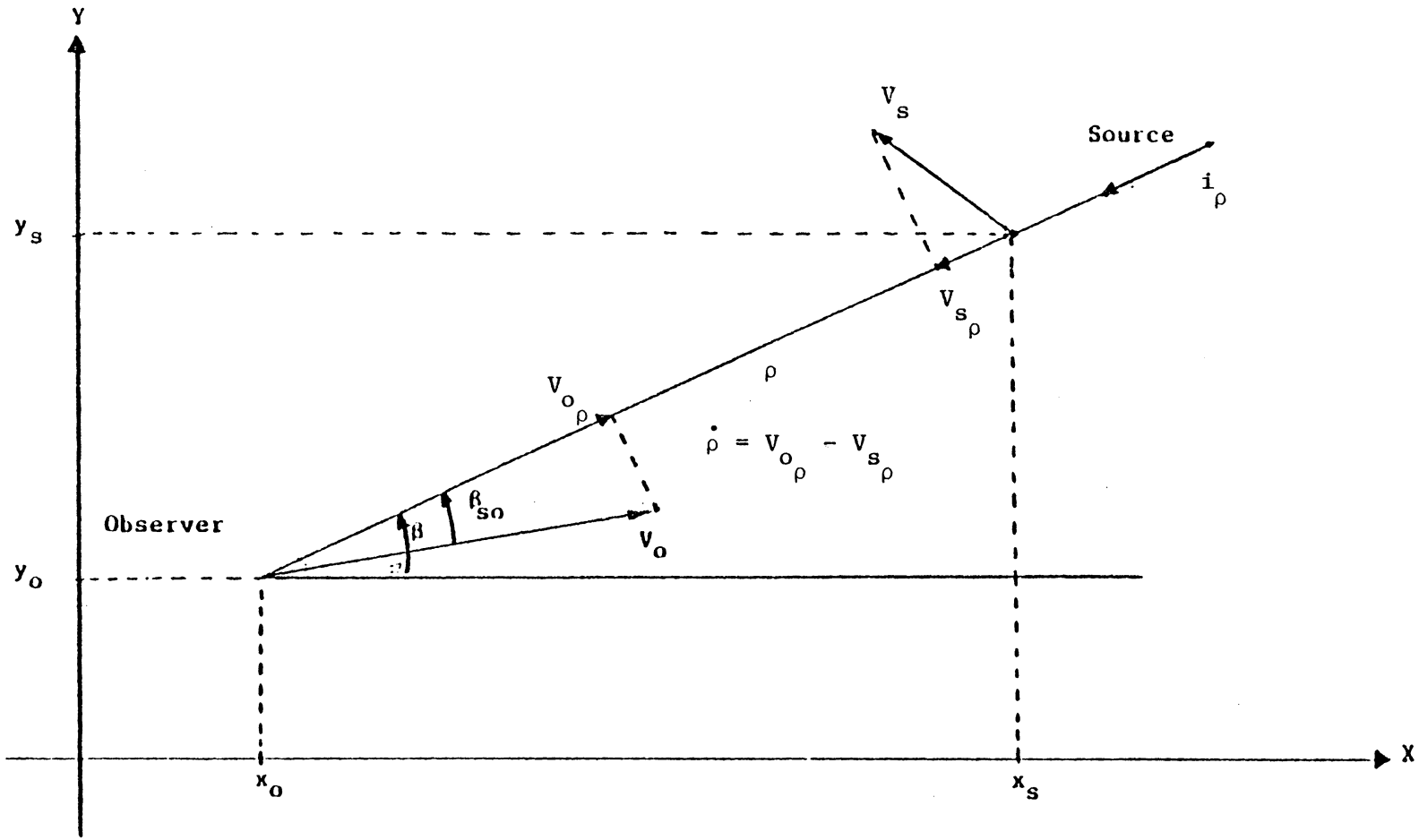

Figure 1.3.1. Geometry of Typical Observer-Source Scenario in the X-Y plane.

Table 1.3.1

Explanation of Parameters Appearing in Figure 1.3.1.

ρ	the polar radius
$\dot{\rho}$	difference between V_{o_ρ} and V_{s_ρ}
i_ρ	unit vector defining the radial direction
V_o	the velocity vector of the Observer
V_{o_ρ}	the Observer velocity in the negative radial direction
V_s	the velocity vector of the Source
V_{s_ρ}	the Source velocity in the radial direction
β	the angle between the polar radius ρ and the (fixed) X axis
β_{so}	the relative bearing of the Source with respect to the Observer
x_o, y_o, x_s, y_s	position coordinates of the Observer and Source, respectively, in the rectangular coordinate system

By exploiting several simplifications provided by the problem's geometry, we arrive at the final state equations.

$$\begin{bmatrix} \rho \\ \dot{\rho} \\ w'_\rho \end{bmatrix}_{k+1} = \begin{bmatrix} 1 & A & B \\ 0 & E & F \\ 0 & 0 & e^{-aT} \end{bmatrix} \begin{bmatrix} \rho \\ \dot{\rho} \\ w'_\rho \end{bmatrix}_k + \begin{bmatrix} C & (A-T) \\ A & (E-1) \\ 0 & 0 \end{bmatrix} \begin{bmatrix} U_s \\ V_o \text{Cos}\beta_{so} \end{bmatrix}_k + \begin{bmatrix} D \\ G \\ J \end{bmatrix} w(k) \tag{1.3.7}$$

or

$$\underline{X}(k+1) = \phi\, \underline{X}(k) + \Gamma\, \underline{U}(k) + \psi\, u(k)$$

Comparison of 1.3.7 and 1.3.5 reveals that target motion in the radial direction is modeled very similarly to that in one rectangular coordinate. Note that w'_x and U_x have been replaced by their equivalents acting in the radial direction w'_ρ and U_s. The state variable equations of 1.3.7 are collectively known as the radial channel model.

One important point which was lost in this abbreviated derivation should be discussed at this time. The exact distance separating an observer and a source is the spherical radius r, which must be measured in three-dimensions. In other words, the depth difference between a target and source must be considered (see Figure 1.3.2). However, z in Figure 1.3.2, the depth difference, is typically much less than ρ due to the limited depth range of modern submarines. Therefore, r is approximately equal to ρ and the two-dimensional polar model developed above will closely approximate the spherical range and range rate. Since r and ρ are approximately equal, these terms shall be used interchangeably through the remainder of this text.

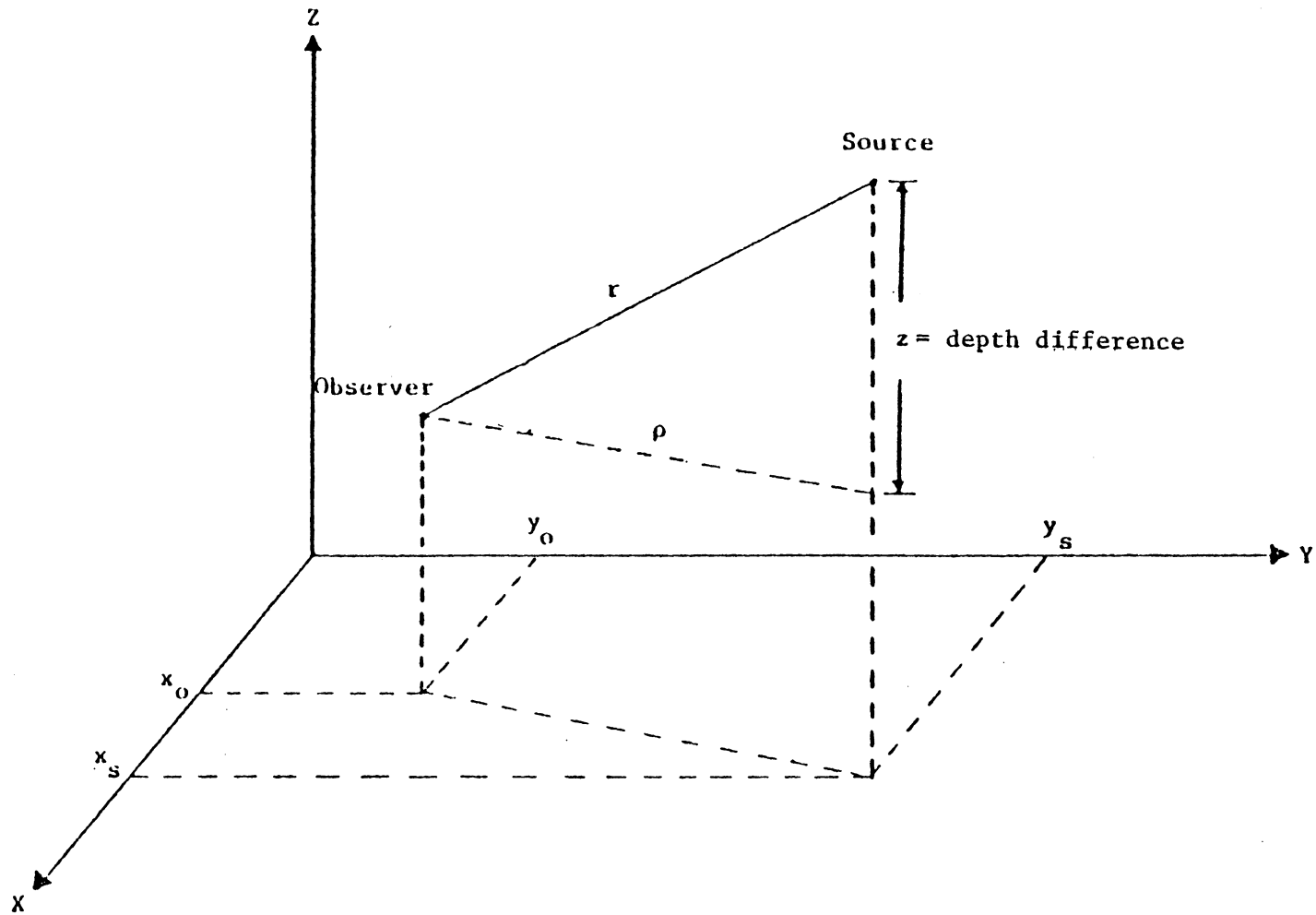

Figure 1.3.2. Geometry of the Observer-Source Scenario in Three Dimensions.

2. DEVELOPMENT OF A SIMPLE RANGE ESTIMATOR USING TIME-DELAY MEASUREMENTS

2.1 Overview

The goal of the next two chapters is to develop a range estimator which will track target motion without prior knowledge of the target status. In the past, this problem has used EKF's to process the nonlinear range measurements. The desire to avoid extended Kalman filtering has inspired a new approach by Moose [2] which uses a nonlinear prefilter to linearize the measurements so that they can be handled by a standard Kalman filter. This chapter will discuss the measurement equations, develop the nonlinear prefilter, and discuss associated simulation results. The next chapter will introduce adaptive filtering concepts and develop an adaptive range tracker.

2.2 Discussion of Time-Delay Measurements

The radial channel model only becomes useful when it can be related to an available set of passive measurements. One measurement commonly selected for ranging problems is that of time-delays. This measurement works well with the radial channel model and can be obtained passively, that is, simply by listening to sounds emitted by the target.

Time-delay measurements, see Figure 2.2.1, consist of two values:

1. τ_1 the difference in propagation times of the direct and surface reflection path.

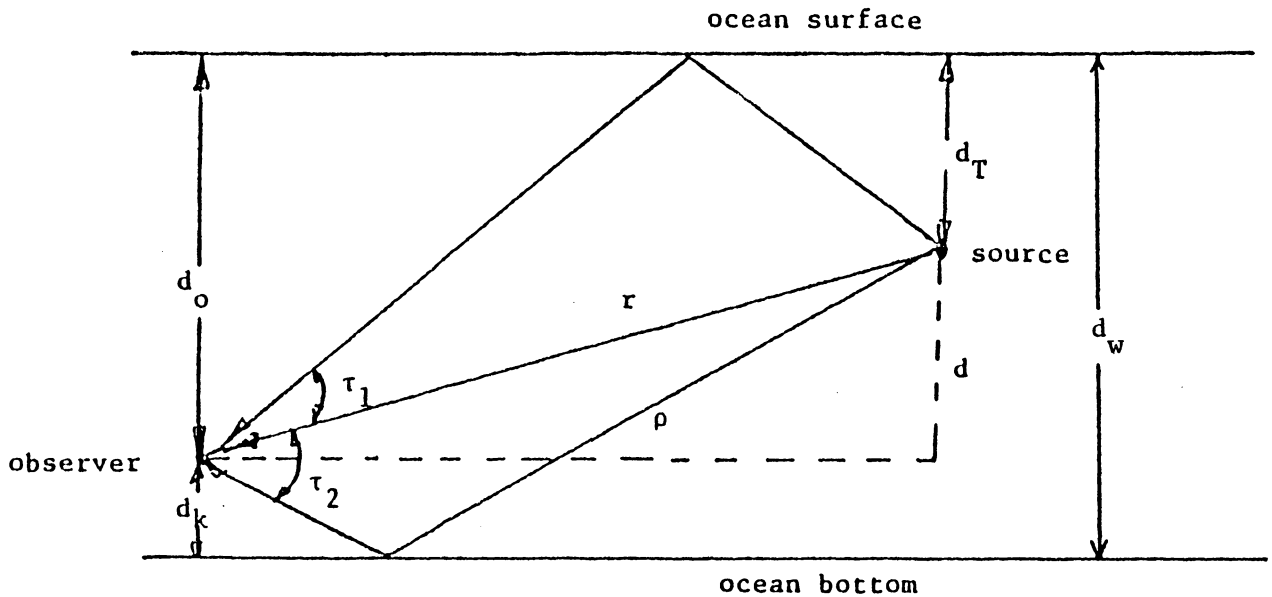

Figure 2.2.1. Geometry of Time-Delay Measurements.

2. τ_2 the difference in propagation times of the direct and bottom reflection path.

Hassab [8] has shown that τ_1 and τ_2 are related to target range ρ and depth d_T in the following way:

$$\tau_1 = \frac{2\, d_o d_T}{\rho C} \tag{2.2.1}$$

$$\tau_2 = \frac{2\, d_k (d_w - d_T)}{\rho C} \tag{2.2.2}$$

These relationships are obviously nonlinear functions of ρ and d_T. In the past, each measurement of τ_1 and τ_2 has been linearized through a Taylor series expansion. This approach requires an EKF, whose disadvantages have been discussed previously, and simultaneous depth and range estimation, which requires a large computational effort. The desire to avoid both of these problems has led to the development of a linearizing prefilter which is discussed in the next section.

2.3 Discussion of the Linearizing Prefilter

The desired prefilter equation, shown in equation 2.3.1, is easily obtained by simultaneously solving equations 2.2.1 and 2.2.2 for ρ.

$$\rho = \frac{b_o}{\tau_1 + a_o \tau_2} \tag{2.3.1}$$

where

$$b_o = \frac{2\, d_o\, d_w}{C}$$

$$a_o = d_o / d_k$$

An equation for d_T can be derived in a similar manner; thereby, providing a means for separate depth and range estimation. In this thesis, we shall only concern ourselves with range estimation. Equation 2.3.1 appears to be a straight-forward method of linearizing ρ, but complications arise when measurement noise is considered.

Realistically, the measurements τ_1 and τ_2 are corrupted by white Gaussian noise processes v_1 and v_2 respectively. When this noise is passed through the nonlinear prefilter [2], it takes on a non-Gaussian distribution v_ρ defined by

$$P(v_\rho) = \frac{\rho\tau_T}{\sigma\sqrt{2\pi}\ (\rho + v_\rho)^2} \exp\left[\frac{-\tau_T^2\ v_\rho^2}{2\sigma^2(\rho + v_\rho)^2}\right] \qquad (2.3.2)$$

where $$\tau_T = \tau_1 + a_o\ \tau_2$$

and the measurement equation at the output of the prefilter is now

$$z_\rho = \rho + v_\rho \qquad (2.3.3)$$

A typical curve of v_ρ is shown in Figure 2.3.1.

Closed form solutions to the integrals required for v_ρ mean and variance calculations could not be found. Therefore, the statistics were examined through simulation. Simulated values of v_ρ were generated and analyzed as is shown in Figure 2.3.2. A limiter is used at the output of the prefilter to prevent infinite variance values. The results are summarized in Table 2.3.1 for several different SNR's. Note the SNR is controlled by σ which is the variance of v_1 and v_2.

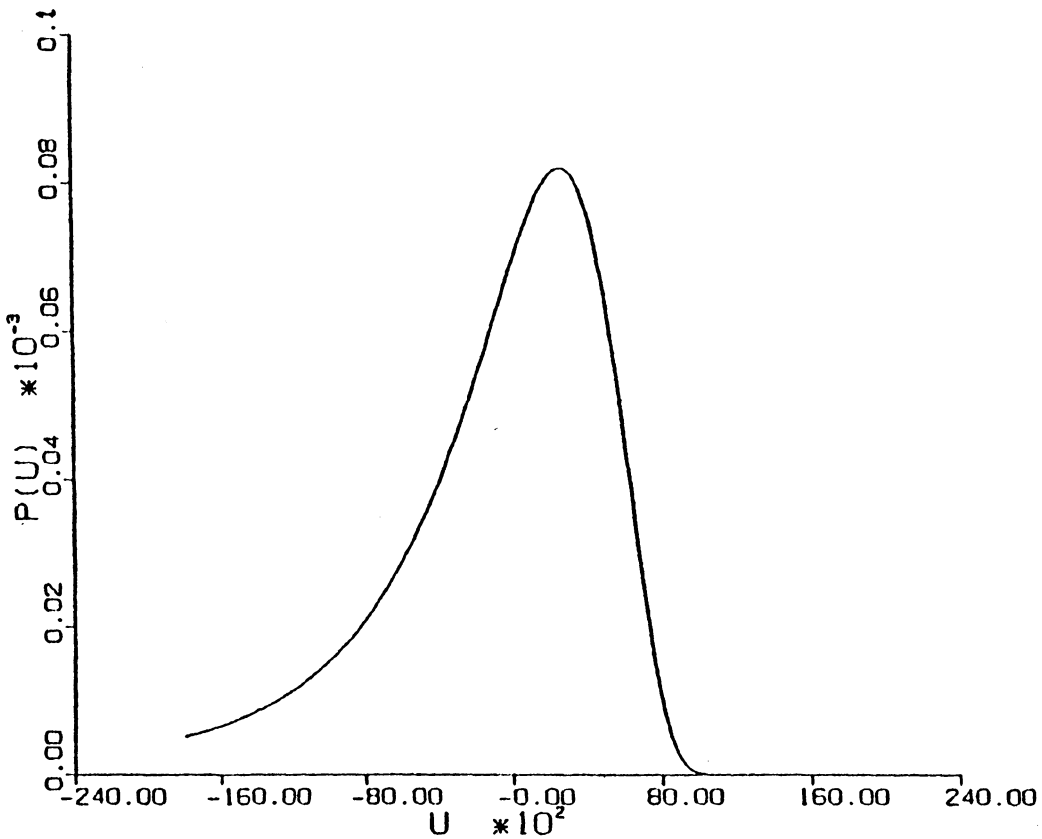

Figure 2.3.1. Typical Distribution of the Measurement Noise at the Prefilter Output.

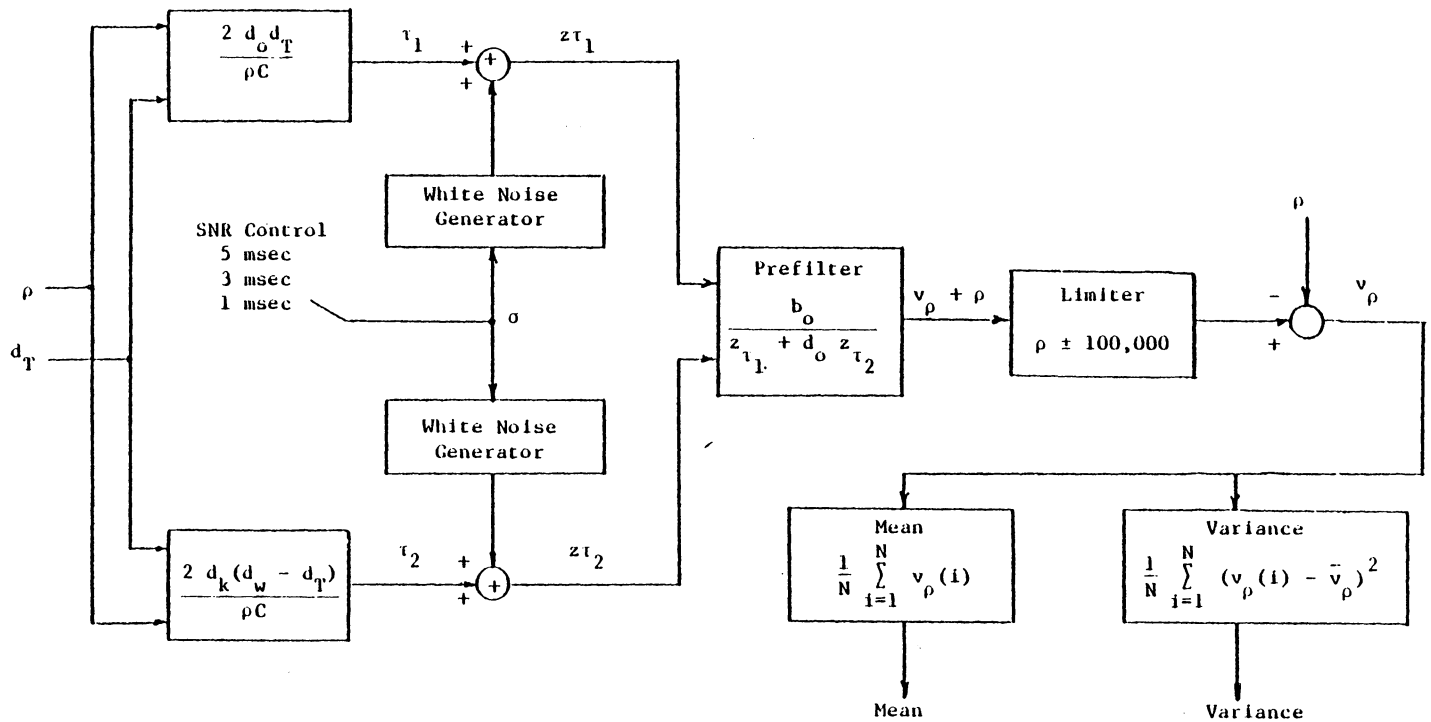

Figure 2.3.2. Block Diagram of v_ρ Mean and Variance Calculation.

Table 2.3.1

Results of Measurement Noise Mean and Variance Calculation

Range in feet	σ = 5msec		σ = 3msec		σ = 1msec	
	Mean	Variance	Mean	Variance	Mean	Variance
95k to 105k	-364.	$.361 \times 10^{10}$	11400.	$.216 \times 10^{10}$	2436.	$.255 \times 10^{9}$
85k to 95k	3545.	$.269 \times 10^{10}$	10300.	$.153 \times 10^{10}$	1766.	$.161 \times 10^{9}$
75k to 85k	6204.	$.190 \times 10^{10}$	8679.	$.103 \times 10^{10}$	1238.	$.972 \times 10^{8}$
65k to 75k	7068.	$.127 \times 10^{10}$	6560.	$.641 \times 10^{9}$	831.	$.553 \times 10^{8}$
55k to 65k	6841.	$.780 \times 10^{9}$	4527.	$.354 \times 10^{9}$	527.	$.290 \times 10^{8}$
45k to 55k	5588.	$.427 \times 10^{9}$	2750.	$.168 \times 10^{9}$	310.	$.137 \times 10^{8}$
35k to 45k	3518.	$.192 \times 10^{9}$	1413.	$.633 \times 10^{8}$	163.	$.552 \times 10^{7}$
25k to 35k	1650.	$.605 \times 10^{8}$	588.	$.179 \times 10^{8}$	72.	$.172 \times 10^{7}$
15k to 25k	487.	$.102 \times 10^{8}$	175.	$.323 \times 10^{7}$	23.	$.336 \times 10^{6}$
5k to 10k	62.	$.549 \times 10^{6}$	24.	$.191 \times 10^{6}$	3.8	$.208 \times 10^{5}$

σ = Standard Deviation of v_1 & v_2

Table 2.3.1 shows that v_ρ has a non-zero mean and a variance which are nonlinear functions of range and SNR. These statistics must be altered for they are not compatible with the Kalman filter that will process the range measurements. For example, v_ρ must be zero mean. This is achieved by a table look-up of the measurement noise mean based on the tracker's previous estimate of ρ and the SNR (see Table 2.3.1). This mean is then subtracted from the current measurement z_ρ producing a zero mean noise process. A similar table look-up method is used to select the proper variance required by the Kalman filter. Simulations have shown that the values in Table 2.3.1 are sufficient to insure measurement compatibility with the Kalman filters.

Numerical integration of the variance expression for v_ρ has shown that the variance at any range is infinite. This explains the limiter used in Figure 2.3.2. A similar limiter is required for z_ρ to make the measurement noise statistics compatible with those of Table 2.3.1. A summary of the measurement compensation schemes is given in Figure 2.3.3.

2.4 Results From a Matched Kalman Filter Range Tracker

With the measurement linearization and compensation complete, z_ρ is ready to be processed by a Kalman filter. The radial channel model provides the basis for the Kalman filter which will track ρ from z_ρ. The Kalman filter equations used throughout this thesis are discussed in Appendix A. A simple matched Kalman filter is first used to test

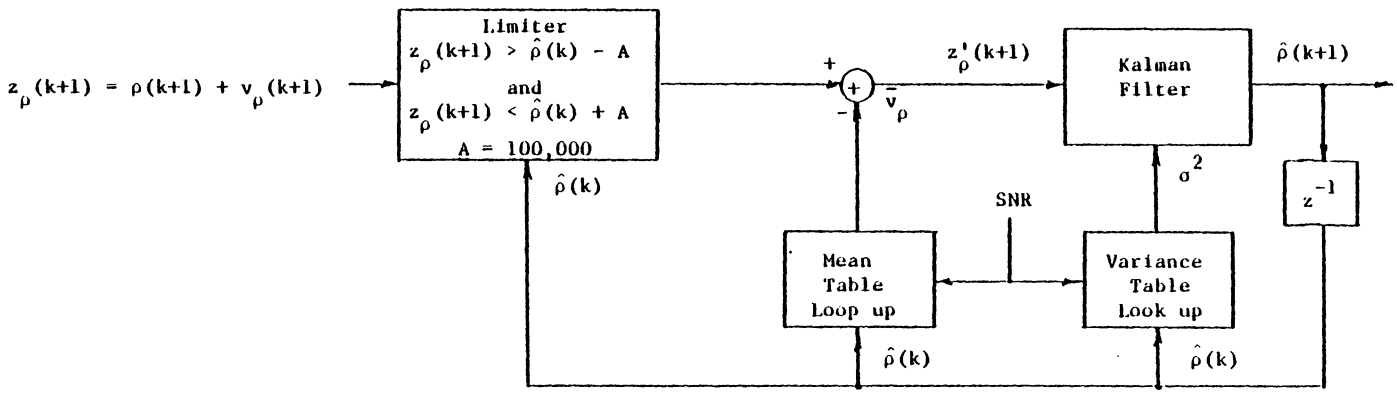

Figure 2.3.3. Block Diagram of Measurement Compensation.

the validity of the compensation schemes. The term "matched" refers to the fact that the Kalman filter knows the value of U_s. Typical results using an approaching-target scenario are shown in Figures 2.4.1 and 2.4.2 for large and small SNR cases respectively.

Before considering the filter performance, one should note the behavior of z_ρ. Both figures demonstrate the reduction in variance of z_ρ as range decreases. Figure 2.4.2 shows particularly well the effect of v_ρ's non-zero mean. The v_ρ values should be evenly distributed around ρ; however, those values of v_ρ larger than ρ have approximately twice the magnitude of those smaller than ρ. There is also quite a difference in the overall variance of z_ρ in the two figures due to the difference in the SNR's. The value of σ is 1msec in Figure 2.4.1 and 5msec in Figure 2.4.2.

The Kalman filter provides very good ρ estimates particularly at close range and when σ is small. These are situations where the SNR is large and one would expect an improvement in tracker performance. The measurement compensations are sufficient to allow convergence of the tracker; however, they are responsible for some of the $\hat{\rho}$ inaccuracies. Other $\hat{\rho}$ errors can be attributed to the non-Gaussian nature of v_ρ. Note that the symbol $\hat{}$ denotes an estimate.

All things considered, the tracker performance is excellent, yet is is useless in its present form. Currently the tracker has, for test purposes, a knowledge of U_s which it would never have in a practical situation. The final tracking system must be able to track the target without knowledge of U_s. One solution to this dilemma is discussed in the next chapter.

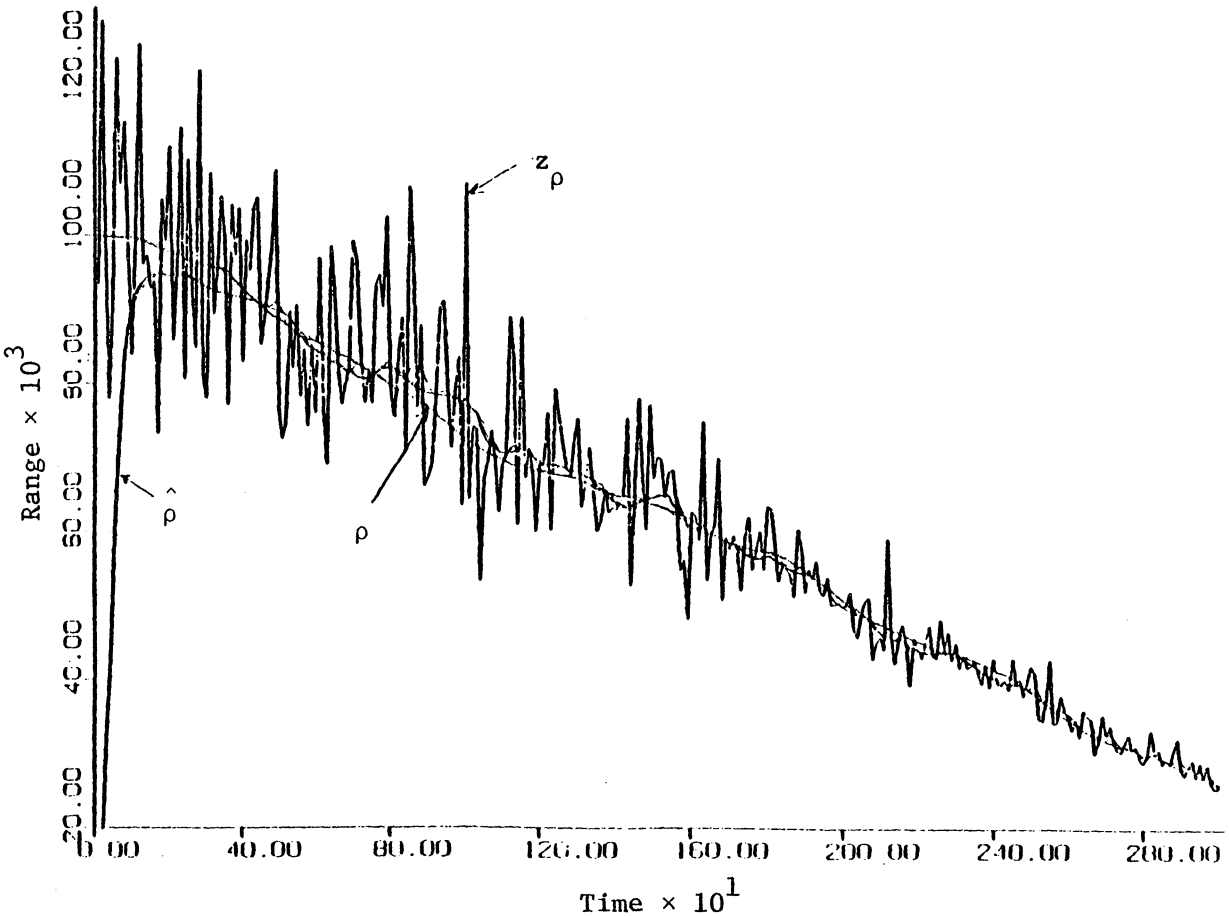

Figure 2.4.1. Range Estimate of Matched Kalman Filter (Large SNR Case).

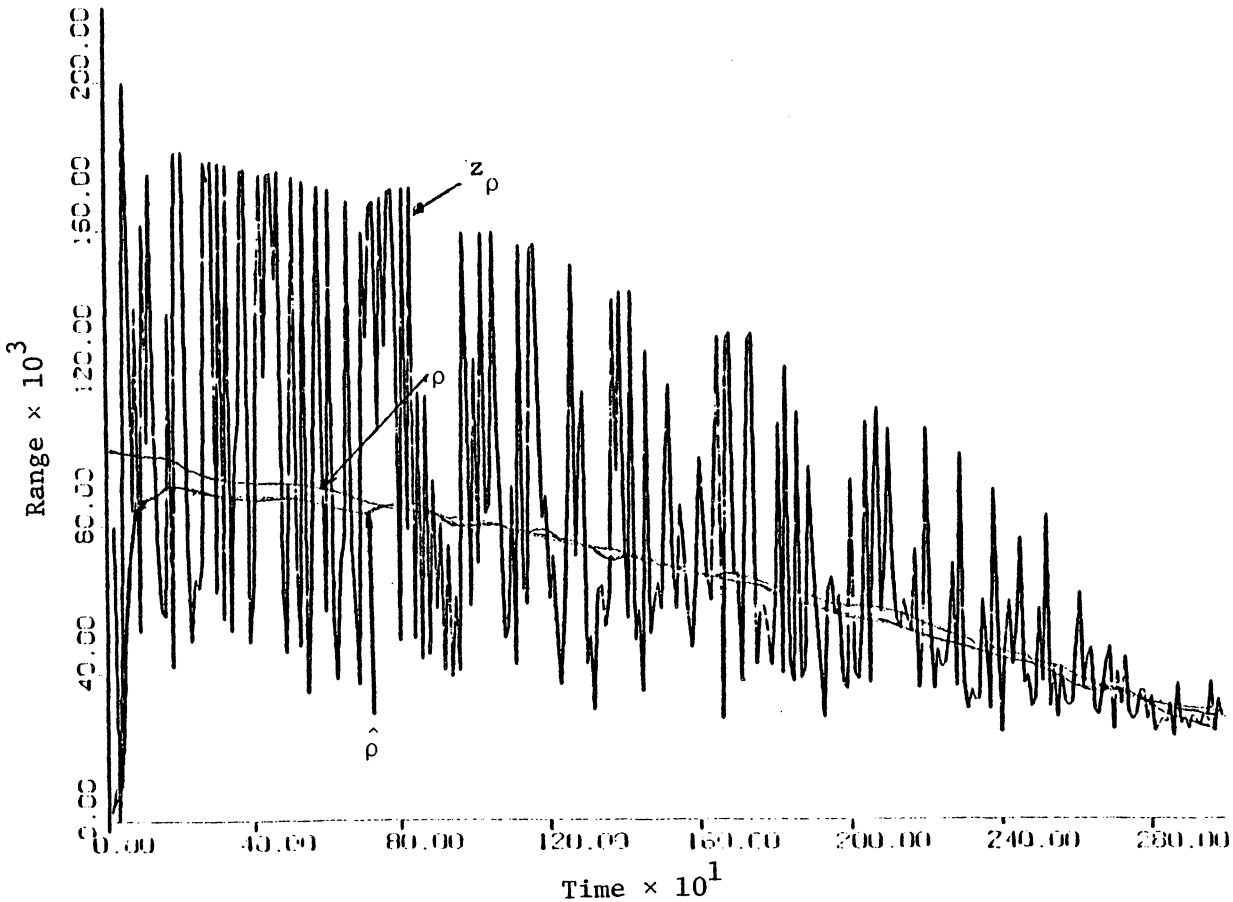

Figure 2.4.2. Range Estimate of Matched Kalman Filter (Low SNR Case).

3. DEVELOPMENT OF AN ADAPTIVE RANGE TRACKER

3.1 Introduction to the Adaptive Filtering Approach

The problem of tracking target range without prior knowledge of U_s can be handled by adaptive state estimation. This involves the use of several tracking filters each conditioned on a different assumed value of U_s. The output of these filters is then adaptively weighted to produce the final unconditional estimate. The mathematical development of basic adaptive filtering techniques is quite complicated and provides little insight into the operation of an adaptive filter. Therefore, we will simply examine the operation of a general adaptive filter from a qualitative view point and then discuss the specific adaptive filter structure to be used for range tracking. The interested reader should refer to Ref. 4 for the complete mathematical development.

To simplify the qualitative explanation, we will assume that the adaptive filter has available only velocity measurements. The target velocity in the polar direction can be represented approximately by a time-correlated Gaussian noise process with a mean U_s. The parameter U_s is related to the target's chosen velocity and the Gaussian distribution accounts for random fluctuations beyond the target's control. This velocity distribution is shown in the top half of Figure 3.1.1.

If the tracking filter knows the value of U_s, as it did in the last chapter, it can readily follow the random fluctuations in velocity around U_s and provide a good estimate of ρ and $\dot{\rho}$. If the filter utilizes a value $U_s^{(i)}$ which is not equal to U_s, it will assume

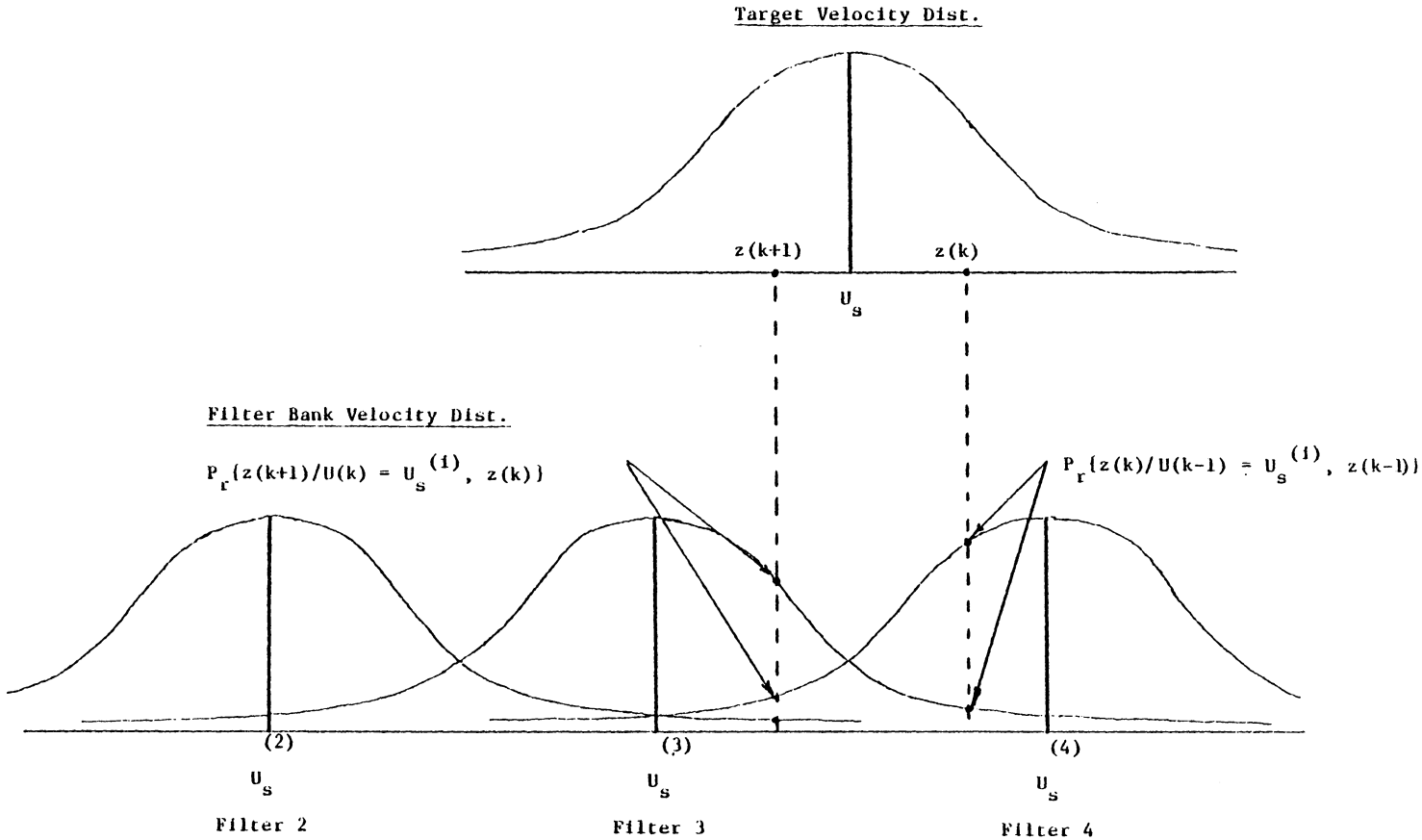

Figure 3.1.1. Target Velocity Distribution vs. Filter Bank Velocity Distribution,

a displaced velocity distribution similar to those of filter 3 or 4 in the lower half of Figure 3.1.1. The mismatched filter follows the random fluctuations in target velocity, but they are assumed to be around a mean of $U_s^{(i)}$ rather than U_s. Therefore, the mismatched filter's output will be similar to that of the matched filter except for a bias proportional to the difference between U_s and $U_s^{(i)}$.

By using several filters, each conditioned on a different value of $U_s(i)$, an overlapping distribution like that in Figure 3.3.1 can be formed. By comparing the target velocity distribution to this overlapping set of distributions, we get a feel for the true value of U_s. For example, we can see that the target velocity distribution in Figure 3.1.1 is located between those of filters 3 and 4. Therefore, U_s is between $U_s^{(3)}$ and $U_s^{(4)}$ and the target velocity will be between the velocity estimates of filters 3 and 4. The final velocity estimate of the adaptive filter is formed by a weighted sum of the filter outputs. The i^{th} weighting factor is related to how close the target velocity distribution is located to that of the i^{th} filter. Therefore, one would expect the weighting factors associated with Figure 3.1.1 to be large and approximately equal for filters 3 and 4 and small for the remaining filters.

To understand the exact calculation of the weighting factors, one must think of the velocity distribution associated with the i^{th} filter (Figure 3.1.1) as being the distribution for the probability that a measurement resulted from a target whose U_s equals $U_s^{(i)}$. This new probability is calculated for each filter every measurement. The

weighting factors are proportional to these probabilities and their sum equals one. For example, the probability of the measurement z(k) (Figure 3.1.1) resulting from a target whose U_s equals $U_s^{(4)}$ is greater than that for any other $U_s^{(i)}$. Therefore filter 4 will receive the largest weighting factor. The probability of the next measurement z(k+1) being from a target whose U_s equals $U_s^{(3)}$ is larger than any other filter, so filter 3 will receive the largest weighting factor.

Since the weighting factors are based on the relationship of the target's U_s to the filters' $U_s^{(i)}$, they should remain constant until U_s changes with respect to the $U_s^{(i)}$'s. However, measurement noise and the random nature of the target velocity cause the measurements to assume different values at each iteration of the tracker even if U_s remains constant. This in turn forces the weighting factors to change value at each iteration. One way to stabilize the weighting factors is to average them. Simulations have proven the viability of this stabilizing approach.

In summary, an adaptive filter consists of several Kalman filters, each conditioned on a different value of $U_s^{(i)}$. The output of each filter is adaptively weighted by a factor proportional to the probability that the received measurement resulted from a target whose velocity distribution is the same as that of the filter in question. The weighting factors are averaged to minimize fluctuations caused by measurement noise. The final unconditional estimate is obtained from the sum of the weighted filter outputs.

The specific adaptive filter to be used, with the range tracker developed in Chapter 2, processes range measurements and consists of six Kalman filters. The value of $U_s^{(i)}$ used by the i^{th} filter is .6 greater than that of the $(i-1)^{th}$ filter. The filter bank spans the entire velocity range of typical targets to insure proper target tracking at any velocity. The weighting factors are expressed mathematically as

$$\begin{aligned} \underline{w}(k+1) &= C(k)P^{*}(k)\Phi^{*T}(k)\underline{w}(k) \\ \bar{\underline{w}}(k+1) &= \frac{1}{N}\sum_{i=k+1-N}^{k+1}\underline{w}(i) \end{aligned} \tag{3.1.1}$$

where

$w(k+1)$ is a 6×1 vector containing the new weighting factors for the six Kalman filters

$C(k)$ is a scalar chosen to make the sum of the weighting factors at time k+1 equal to one

$P^{*}(k)$ is a 6×6 diagonal matrix. The (i,i) element is the probability that a measurement resulted from a target whose $U_s = U_s^{(i)}$.

Φ^{*T} is a 6×6 matrix which models the semi-Markov nature of a maneuver. The (i,i) element is the probability that the target will remain in the i^{th} velocity state. The (i,j) element is the probability that the target will change from the i^{th} to the j^{th} velocity state. The sum of the elements in each row or column must equal one.

w(k) is a 6×1 vector containing the previous weighting factors.

* the asterisk is used to reduce confusion between P and Φ used in the Kalman filter equations of Appendix A.

These weighting factors are computed in basically the same manner as were those described earlier in this section, with the exception of the Φ^{*T} term. This matrix defines the probabilities of various target maneuvers which are considered to have semi-Markov statistics. Typical probabilities used in Φ are .8 for maintaining the same velocity and .04 for any change in velocity. These values typically remain constant for an entire scenario.

The Gaussian probability distribution used to calculate P(i,i) is

$$P^{*}_{(i,i)} = e^{-1/2 \frac{\tilde{Z}^2}{V}} \qquad (3.1.2)$$

where $\tilde{Z} = z(k+1) - H(\phi \hat{\underline{x}}(k) + \Gamma U_s^{(i)})$

$V = (HM(k+1)H^T + R)$

The values of $\tilde{Z}$ and V are easily obtained from each of the Kalman filters in the filter bank. See Appendix A for an explanation of the terms in Equation 3.1.2 and their relationship to Kalman filtering. The value of V is the same for all of the filters; therefore, it need only be calculated once.

3.2 Performance Analysis of the Adaptive Range Tracker

The adaptive filter discussed in the last section forms the basis

for an adaptive range estimator which can track a target without knowing U_s. A block diagram of the complete range tracker is shown in Figure 3.2.1. From this figure, we see that the Kalman filters have been separated into gain and conditional range estimate sections. The gain section is the same for all of the filters and only needs to be calculated once per measurement. The conditional range estimate section is different for each filter and must be calculated six times per measurement; once for each filter. We also see that the input measurements are averaged. This is done to Gaussianize the input noise distribution via the Central Limit Theorem. The number of input samples averaged is kept small, 10 or less, to minimize unwanted correlation effects.

A simple first order digital filter of the form

$$\hat{\rho}_s(k+1) = a\hat{\rho}_s(k) + b\hat{\rho}(k+1) \qquad (3.2.1)$$

is used to smooth out unwanted fluctuations in the range estimate. Since this filter is also used with all subsequent adaptive filters, the cumbersome subscript s, for smoothed, will be dropped and the symbol ^ will henceforth designate the final estimate whether it is smoothed or not. It should be clear from the text and figures when a smoothing filter is used.

Typical simulation results from the range tracker are shown in Figures 3.2.2 through 3.2.4. The noise has been left out of these plots for clarity. The scenario used to generate the figures starts with the target at a range of 50,000 ft. approaching the stationary

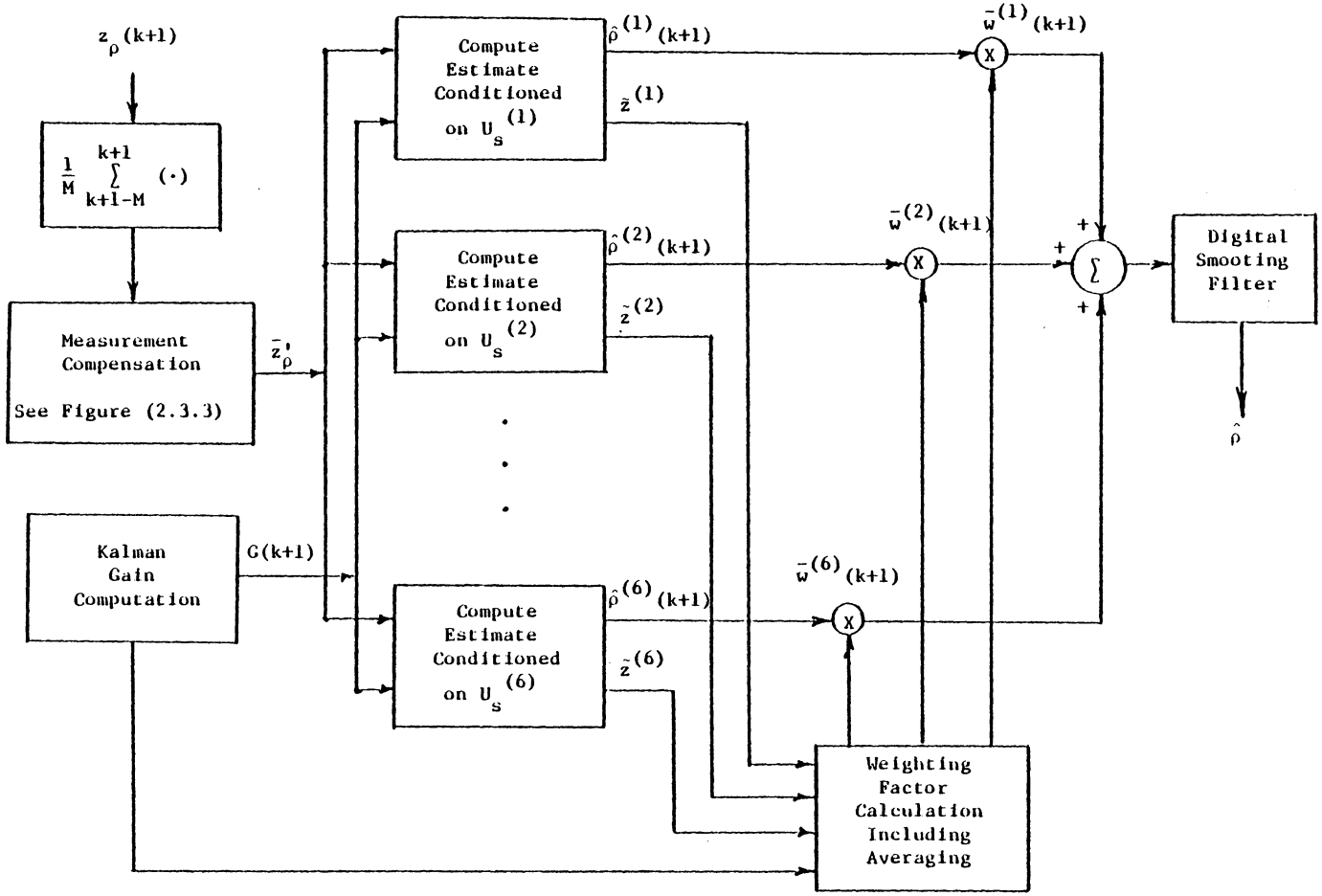

Figure 3.2.1. Block Diagram of Adaptive Range Tracker.

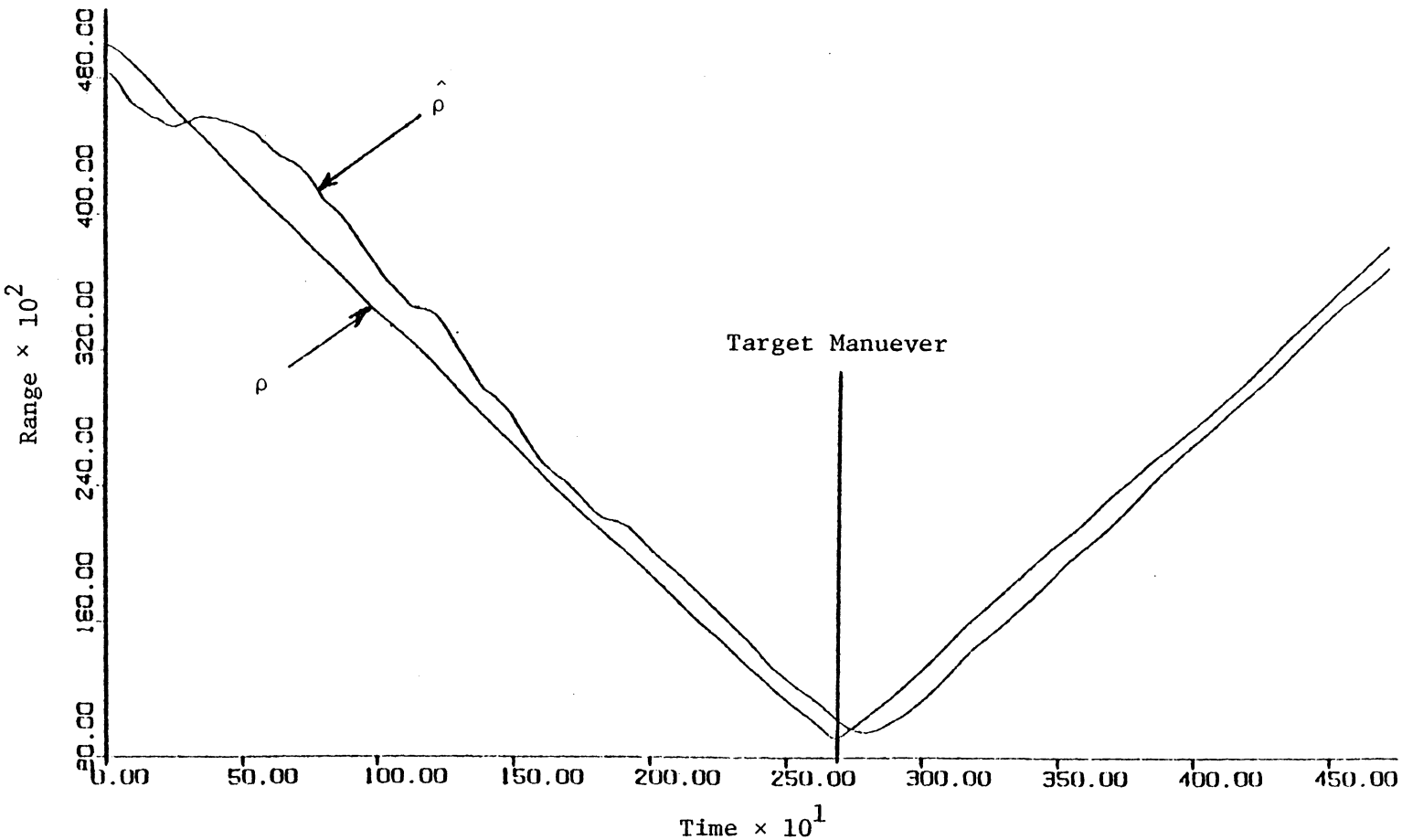

Figure 3.2.2. Range Estimate of the Adaptive Range Tracker.

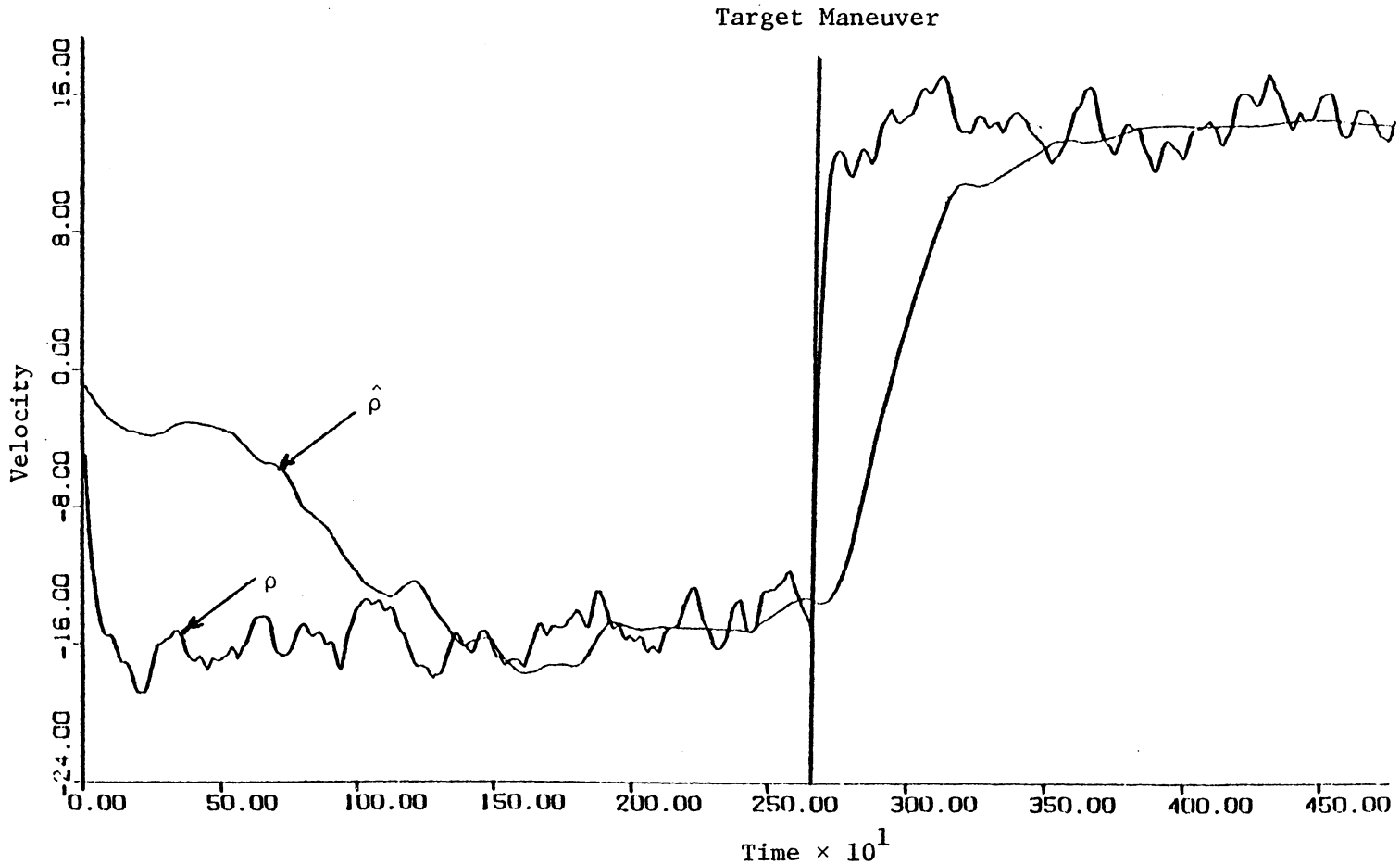

Figure 3.2.3. Velocity Estimate of the Adaptive Range Tracker.

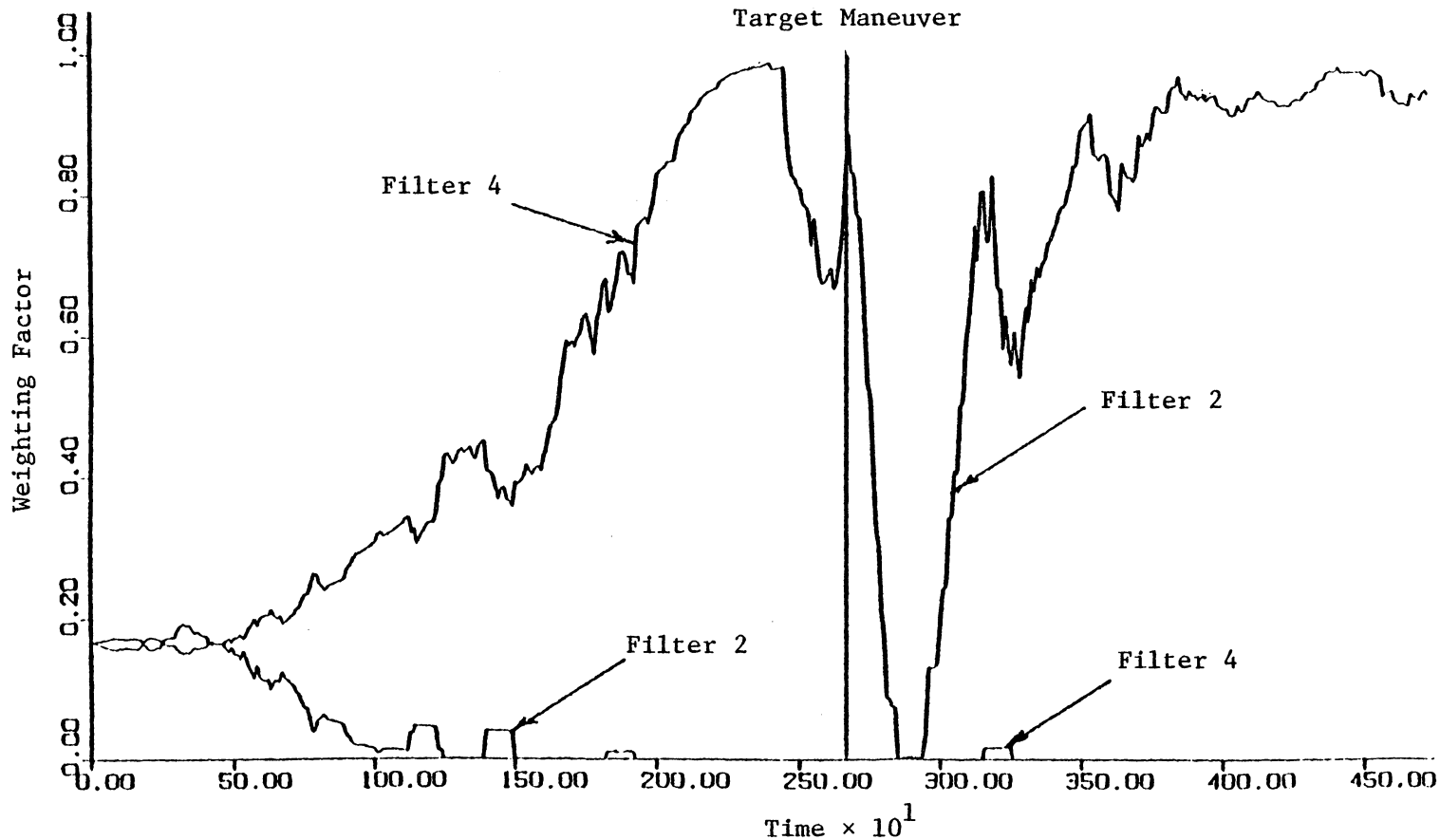

Figure 3.2.4. Illustration of Weighting Factor Behavior.

observer at -15 ft/sec (negative sign denotes an approaching velocity). After approximately 43 minutes, the target abruptly changes its velocity to +15 ft/sec. The measurements in these figures are averaged over 10 samples and the weighting factors are averaged over 30 samples. The sampling time is 10 sec. and the value of σ is 3 msec. The digital filter coefficients a and b are .7 and .3 respectively.

Figure 3.2.2 shows that the range estimate converges quickly and maintains track even through the abrupt maneuver. There is a slight lag time in $\hat{\rho}$ due to the compensation, averaging and smoothing required to obtain the desired $\hat{\rho}$ form. This lag time is considered an acceptable trade off for the more desirable quality of a smooth estimate. While judging these plots, one must keep in mind that the adaptive tracker has no information about U_s, as did the matched Kalman filter of Chapter 2. Yet, the adaptive tracking results are quite good and comparable to those of the matched tracker. The fact that the results from these two filters are indeed comparable greatly supports the validity of the adaptive filtering approach.

Figure 3.2.3 illustrates the performance of the velocity estimate provided by the range tracker. The velocity estimate converges rather slowly and tends to track the average rather than the instantaneous target velocity. The performance of the velocity tracker can be improved by changing various parameters of the tracker such as the number of measurements and/or weighting factors averaged. But, this tracker is primarily designed to produce the best estimate of range and not velocity. Therefore, we must accept the velocity estimate as

is, which is not band considering its secondary role. A tracker designed specifically for velocity estimation will be developed in later chapters.

The third plot in this group is included to provide some insight into the operation of the adaptive filter. The two values of U_s used in this scenario are -.6 and .6 chronologically. These values correspond to the values of $U_s^{(i)}$ used by filter 4 and filter 2 of the adaptive filter bank respectively. Before the maneuver, we would expect the weighting factor of filter 4 to approach one while that of filter 2 approaches zero. After the maneuver, the weights should switch values. Figure 3.2.4 illustrates that the weighting factors behave exactly as expected.

The scenario used in these three figures incorporates values of U_s which exactly match the $U_s^{(i)}$'s of the filter bank. However, the target's U_s need not be restricted to only the values of $U_s^{(i)}$. This scenario was selected to insure a good plot of the weighting factors' behavior. The tracker performs well with any value of U_s between two consecutive values of $U_s^{(i)}$. The performance is similar to that shown in the previously discussed figures, so no new plots have been included.

3.3 Conclusion

The desire for a range estimator which can track a target at any velocity and do so with regular rather than extended Kalman filters has led to the adaptive range estimator discussed in this chapter.

The nonlinearities of time-delay measurements are handled by a linearizing prefilter and several measurement compensation schemes. Adaptive filtering techniques allow estimation of target range and velocity regardless of the target's value of U_s. The performance of the adaptive tracker is quite good though the velocity estimate could be improved. A different approach to velocity tracking will be explored in the next two chapters in an attempt to provide an independent source of velocity estimates.

4. INTRODUCTION TO PASSIVE TRACKING USING FREQUENCY MEASUREMENTS

4.1 Introduction

In the first chapters of this thesis, range and range rate were estimated from time-delay measurements. These measurements provide good results, but are not always available, for source and observer maneuvers can change the signal propagation paths in such a way as to prevent their convergence at the observer. Therefore, time-delay measurements should not be depended upon as a sole source of information. Fortunately, a submarine provides other measurable signals whose information can be exploited to back up and/or complement that provided by the time-delay measurements. For example, frequencies generated by rotating machinery on board the submarine contain range rate information derived from the Doppler effect. Consequently, frequency measurements can provide the desired "independent" method of determining range rate. This chapter will discuss the Doppler effect and the use of frequency measurements in a simple passive tracking scheme.

4.2 Fundamental Doppler Principles

Simply stated, the Doppler effect is the observed frequency shift of a signal during a change in the relative position between an observer and a signal source. Mathematically, the frequency shift is

$$\Delta f = -f_o \dot{\rho}/C \qquad (4.2.1)$$

where f_o, $\dot{\rho}$, and C are the center frequency or actual signal frequency,

relative radial velocity and speed of sound in water respectively. This frequency shift added to the center frequency yields f_t the frequency seen by an observer.

$$f_t = f_o + \left(\frac{- f_o \dot{\rho}}{C} \right) = f_o(1 - \dot{\rho}/C) \qquad (4.2.2)$$

Strictly speaking, equation 4.2.2 applies only to the case of a stationary source with a moving observer and not to the case of a stationary observer with a moving source. However, it can be shown that equation 4.2.2 is valid for the latter case if the speed of the source is much less than C as is the case for submarines [9].

To be useful, equation 4.2.2 must also apply to the typical case of a moving observer and source. The exact mathematical formula for this case is

$$f_t = f_o \left(\frac{1 \pm \frac{V_o}{C}}{1 \mp \frac{V_s}{C}} \right) \qquad (4.2.3)$$

where V_s and V_o are the source and observer velocity respectively and the upper (lower) signs imply a converging (diverging) relative range rate. By assuming that V_s and V_o are much less than C, equation 4.2.3 will simplify to equation 4.2.2 [9]. Since the assumptions on V_s and V_o are valid for underwater scenarios, equation 4.2.2 represents the observed Doppler-shifted frequency for all cases of observer-source motion.

Examination of equation 4.2.2 reveals that an approaching (diverging) source with a negative (positive) range rate produces an

observed frequency which is greater (less) than the center frequency. The effect of the range rate sign on f_t is easily seen by the stationary observer of an approaching train sounding its whistle. As the train passes the listener, the range rate changes from negative to positive and the observed whistle frequency changes from f_o plus Δf to a lower frequency of f_o minus Δf.

The most important result of equation 4.2.2 is that it expresses an observed frequency in terms of the desired quantity range rate. If f_o is known, the observed frequency is simply a linear function of the range rate. This simple case is examined in the next section.

4.3 Velocity Tracking Using the Doppler Effect With Known Constant Center Frequency

The tracking problem is greatly simplified if the center frequency is completely known. Unfortunately, this is rarely the case. The center frequency typically consists of a known constant component f_c and an unknown random component f_r. Before examining the case where f_o is the sum of f_c and f_r, we will examine the simpler case where f_o is constant and equal to f_c. These two cases are referred to as the random center frequency (RCF) and constant center frequency (CCF) problems respectively. Examination of the CCF tracker will provide a foundation for the development of an RCF tracker.

To develop the CCF tracker, we must make the assumption that an estimate of f_c is available from time-delay or bearing measurements. Since f_o equals f_c which is constant and known, f_o can be considered as a bias and subtracted from both sides of equation 4.2.2 to yield 4.3.1

$$\Delta f(k+1) = \left[\frac{-f_o}{C}\right] \dot{\rho}(k+1) \qquad (4.3.1)$$

Now the measurement is simply the Doppler shift and is linearly related to the state variable range rate. By using a reduced order version of the radial channel model from Chapter 1 to estimate $\dot{\rho}$, the Doppler shift can be passively tracked by a Kalman filter with the following measurement equation

$$z_f(k+1) = \Delta f(k+1) + v(k+1) = \begin{bmatrix} \frac{-f_o}{C} & 0 \end{bmatrix} \begin{bmatrix} \dot{\rho} \\ w_f' \end{bmatrix}_{k+1} + v(k+1) \qquad (4.3.2)$$

$$z_f(k+1) = Hx(k+1) + v(k+1)$$

where the reduced order radial channel model is

$$\begin{bmatrix} \dot{\rho} \\ w_f' \end{bmatrix}_{k+1} = \begin{bmatrix} E & F \\ 0 & e^{-aT} \end{bmatrix} \begin{bmatrix} \dot{\rho} \\ w_f' \end{bmatrix}_k + \begin{bmatrix} A & (E-1) \\ 0 & 0 \end{bmatrix} \begin{bmatrix} U_s \\ V_o \end{bmatrix}_k + \begin{bmatrix} G \\ J \end{bmatrix} w_f(k) \qquad (4.3.3)$$

A white Gaussian noise term v(k+1) has been added to equation 4.3.2 to model measurement noise.

The integrity of this model is shown in Figure 4.3.1 where the Kalman filter is matched to the plant (i.e. the Kalman filter knows the value of U_s). Noise is not shown in this nor the remaining velocity plots for it is in terms of frequency not velocity. However, Figure 5.3.4 does provide some insight into the scope of frequency noise.

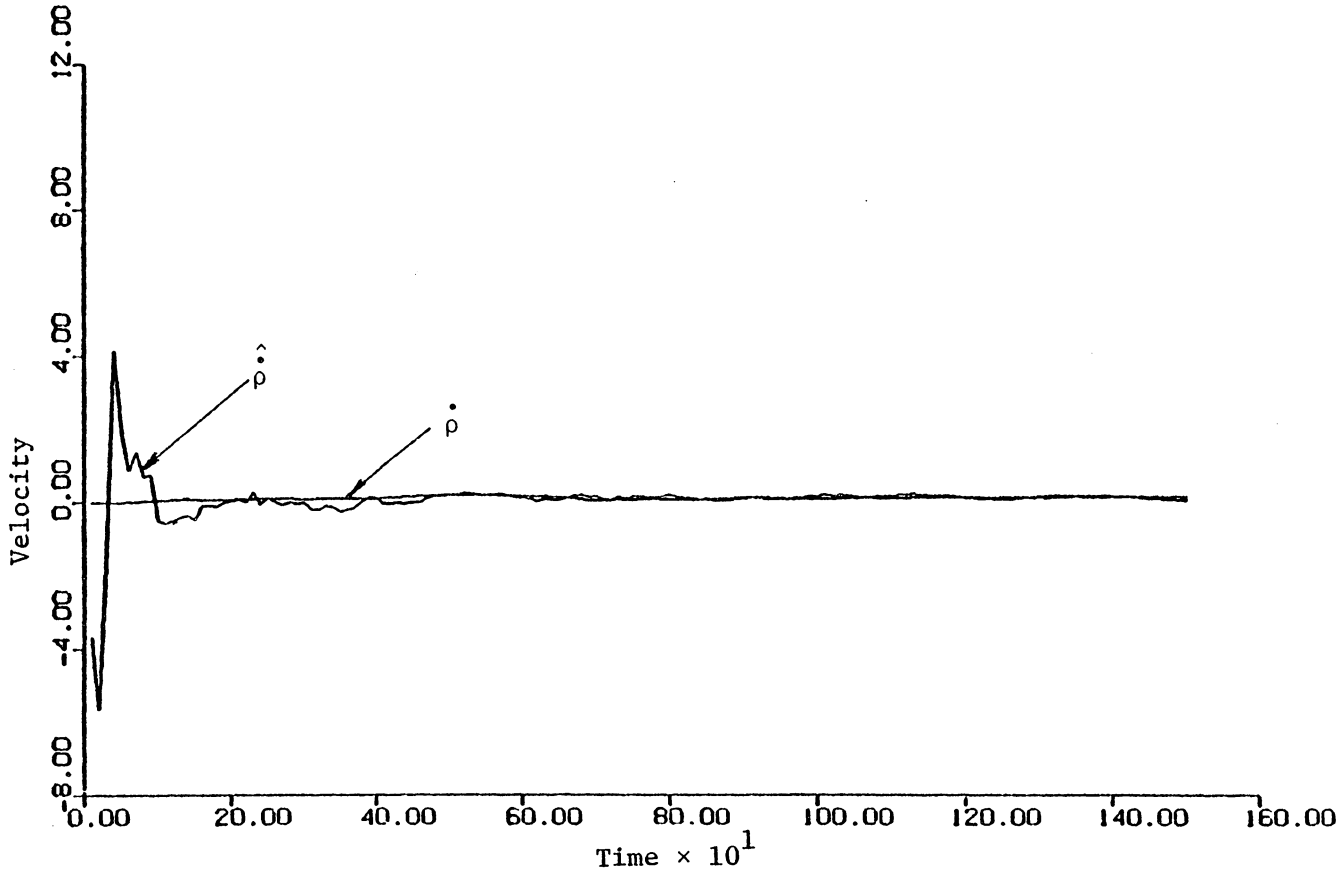

Figure 4.3.1. Velocity vs. Velocity Estimate of a Matched Kalman Filter Using a Constant Center Frequency Scenario.

The velocity of the observer and source in Figure 4.3.1 are both 5 ft/sec. Therefore, their relative range rate is equal to zero. The initial estimate is set equal to the relative range rate in this and all subsequent plots. The sampling time is 10 sec. and the variance of v(k+1) is 0.09. A block diagram of the plant model used in this and all subsequent plots is shown in Figure 4.3.2. This figure also defines some important parameter values.

The Kalman filter output converges quickly and produces an excellent estimate of the plant velocity. Though the matched Kalman filter demonstrates the validity of the state model, it is useless in practical situations. As with the range estimator the final velocity tracker must be able to track a target's velocity without prior knowledge of U_s. Therefore, we must expand the current tracker to an adaptive format like that used with the time-delay measurements.

To this end, six Kalman filters, each conditioned on a different value of U_s, are used to adaptively track the frequency measurements. The filters are separated in velocity by 10 ft/sec and are adaptively weighted in the same manner as are the time-delay filters. The unconditional velocity estimate is smoothed by the first order digital filter of equation 3.2.1 with a and b equal to .9 and .1 respectively. Note that no input averaging or compensation is required due to the zero-mean Gaussian statistics of the measurement noise. Typical results from the adaptive frequency tracker are shown in Figure 4.3.3 where: V_o is 5 ft/sec, V_s is -13.75 ft/sec, the sampling time is 10 seconds and the variance of v(k+1) is 0.09.

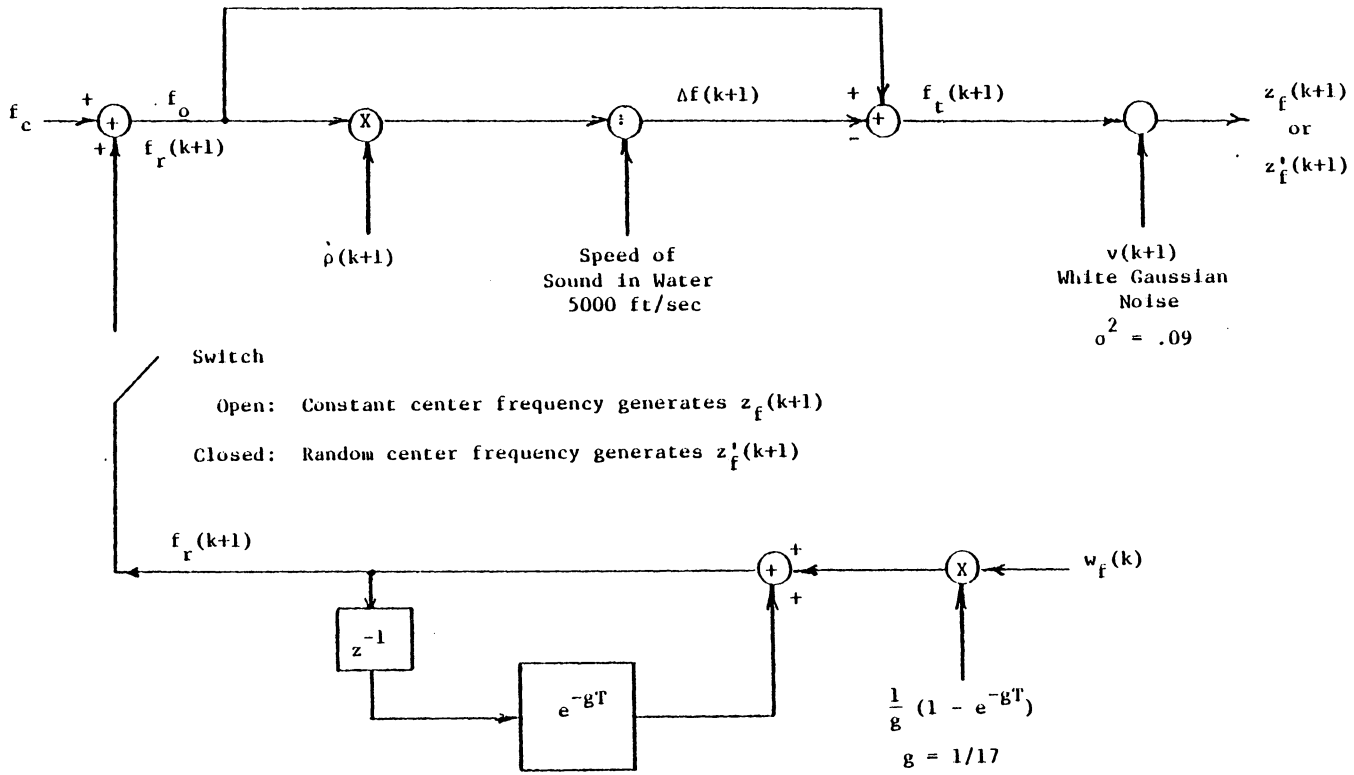

Figure 4.3.2, Block Diagram of Frequency Measurement Generation.

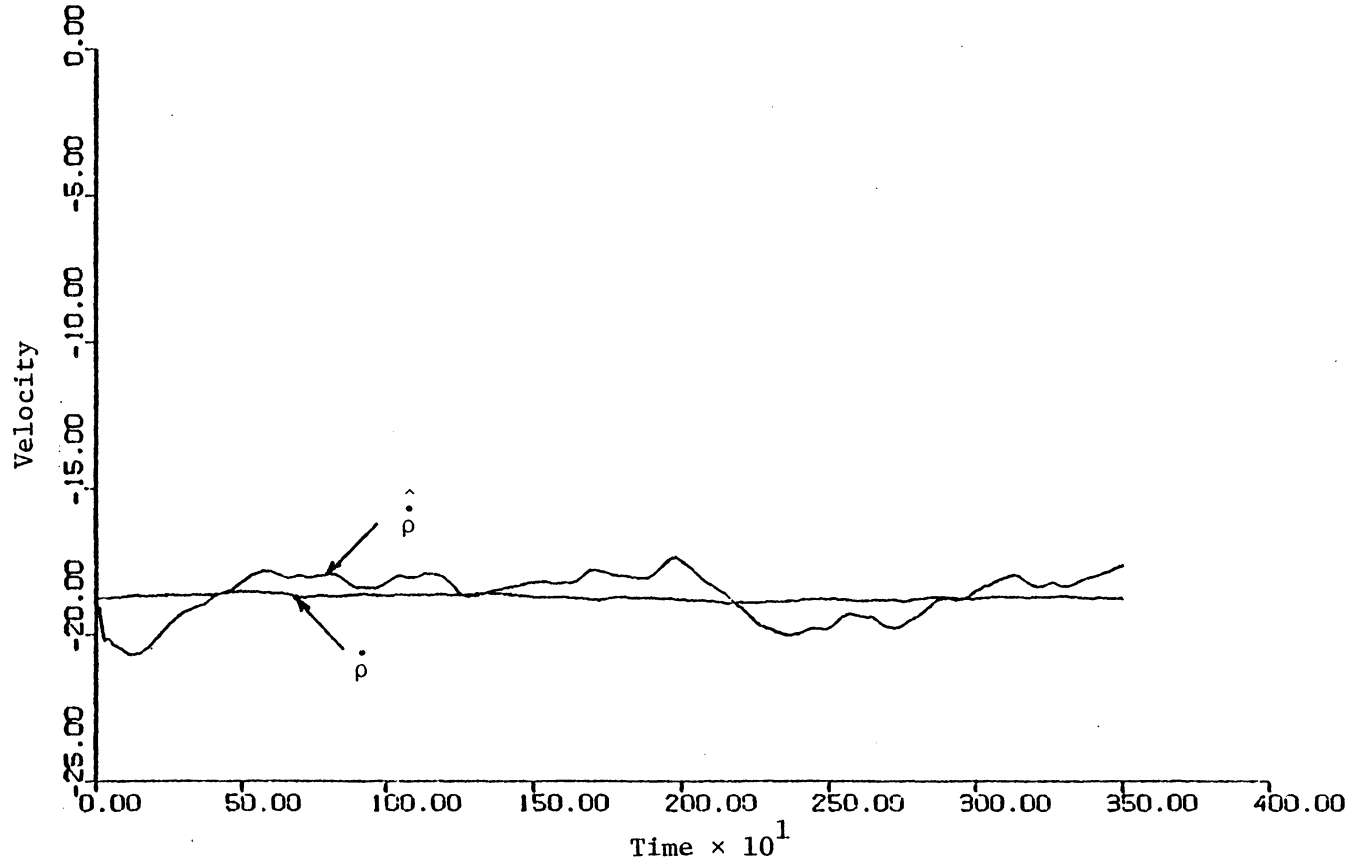

Figure 4.3.3. Velocity vs. Velocity Estimate of an Adaptive Kalman Filter with Constant Center Frequency Scenario.

Before examining Figure 4.3.3, one must consider the following observations. The lack of information about U_s causes a greater degree of error in the estimate of the adaptive filter then in that of the matched filter. Some of the errors could be reduced by fine tuning various parameters of the filter to increase tracking performance. However, a great deal of time and computer funds can be expended in the fine tuning process which is generally only attempted with real data anyway. And finally, some of the errors seen in Figure 4.3.3 can be attributed to inaccuracies in the Gaussian random variable generator used in the simulation. Therefore, we shall be satisfied to simply demonstrate that the adaptive tracker provides reasonable estimates and is consequently a valid approach to the problem. Keeping the above in mind, the results of Figure 4.3.3 are quite reasonable and demonstrate the validity of the adaptive tracking approach.

With the integrity of the constant center frequency tracker now demonstrated, we are in a position to attack the random frequency tracking problem. If a Kalman filter can be developed to estimate the random variation around the mean of f_c, this estimate can be subtracted from the current frequency measurement yielding the constant center frequency problem discussed in this chapter. Efforts to this end are discussed in the next chapter.

4.4 Conclusions

The need for information to backup the time-delay measurements can be fulfilled by frequency measurements with the use of the Doppler

effect. In the case where the center frequency is known and constant, the velocity tracking problem is straightforward and utilizes the adaptive techniques developed for time-delay measurements. The adaptive frequency tracker developed for the constant center frequency problem provides good results and is also a foundation for the development of a random center frequency tracker.

5. PASSIVE TRACKING USING THE DOPPLER EFFECT WITH A RANDOM CENTER FREQUENCY

5.1 Introduction

To address the realistic passive velocity tracking problem, one must consider the center frequency to consist of both a constant and random component as shown in equation 5.1.1.

$$f_o = f_c + f_r \tag{5.1.1}$$

where f_o, f_c, f_r are respectively the center frequency seen by the observer, the constant portion of f_o, and the random portion of f_o. The center frequency is produced by rotating machinery on board the submarine. Ideally this machinery should produce a constant frequency f_o, but temperature fluctuations, changes in load, etc. cause the random fluctuations, f_r, and consequently the random center frequency f_o.

We are assuming that f_c is known, so we are faced with the problem of estimating f_r, If this can be achieved, the random center frequency problem will simplify to one of constant center frequency tracking by merely subtracting the f_r estimate from the current frequency measurement. Development of a f_r tracker is based on work done by Moose and McCabe [9] and is discussed in the next section.

5.2 Development of a Random Center Frequency Estimator

To fully understand the required structure of the f_r tracker, we must take a closer look at the measurements the tracker will use.

Remembering that the frequency measurement is the sum of the Doppler shift and the center frequency, we can write

$$z_f' = f_c + f_r + \Delta f + v \tag{5.2.1}$$

using equation 5.1.1 and neglecting the (k) time notation. We assume f_c is constant and known so that it can be subtracted from both sides of 5.2.1 to yield the measurement available to the f_r tracker.

$$z_f'' = f_r + \Delta f + v \tag{5.2.2}$$

By neglecting noise, we can define the underlying process as:

$$f_o' = f_r + \Delta f \tag{5.2.3}$$

The significance of equation 5.2.3 is that the quantity we wish to track, f_r, is not only corrupted by noise, but also by an unknown bias Δf. The selected f_r tracker will be a Kalman filter whose state variable model must be able to estimate f_r as a zero mean process regardless of the bias Δf. Simulations using various state variable structures have shown that a two-dimensional state model provides the best results. The first state variable tracks f_o' and forces the second state variable to maintain a zero mean while tracking only f_r.

The required state equations can now be developed with the assumptions that the distribution of f_r is Gaussian with zero mean and the autocorrelation function of f_o' is

$$R_{f_o'}(\tau) = (\Delta f)^2 + \sigma^2 \, e^{-g|\tau|} \tag{5.2.4}$$

where g is the correlation time constant. This autocorrelation function was selected for it, "provides a tractable yet realistic model for actual random phenomena," [9] and it allows for bandwidth selection using the parameter c. We also assume that the target maintains a constant velocity profile for long periods of time so that Δf in equation 5.2.4 can be considered constant. This assumption is valid for most underwater scenarios and will prove to be quite useful in later simulations.

Since f_r is simply modeled as a correlated white noise process, its state variable equation can easily be expressed in discrete form as

$$f_r(k+1) = e^{-gT} f_r(k) + \frac{1}{g} (1 - e^{-gT}) w_f(k) \qquad (5.2.5)$$

where w_f is a zero mean white noise process and g is the correlation time constant. To obtain the state equation for f_o' we substitute equation 5.2.5 into equation 5.2.3 to yield

$$f_o'(k+1) = \Delta f(k+1) + e^{-gT} f_r(k) + J w_f(k) \qquad (5.2.6)$$

where

$$J \equiv \frac{1}{g} (1 - e^{-gT})$$

Equation 5.2.6 is not yet a valid state equation for Δf is unknown. This problem is easily handled by noting that

$$\Delta f(k) = f_o'(k) - f_r(k) \qquad (5.2.7)$$

and

$$\Delta f(k) \cong \Delta f(k+1)$$

By substituting this into 5.2.6, we obtain

$$f_o'(k+1) = f_o'(k) + (e^{-gT} - 1)\, f_r(k) + J\, w_f(k) \qquad (5.2.8)$$

Equations 5.2.8 and 5.2.5 constitute the state variable model used by the f_r tracker. These equations are shown in matrix form below.

$$\begin{bmatrix} f_o' \\ f_r \end{bmatrix}_{k+1} = \begin{bmatrix} 1 & (e^{-gT} - 1) \\ 0 & e^{-gT} \end{bmatrix} \begin{bmatrix} f_o' \\ f_r \end{bmatrix}_k + \begin{bmatrix} J \\ J \end{bmatrix} w_f(k) \qquad (5.2.9)$$

$$z_f''(k+1) = \begin{bmatrix} 1 & 0 \end{bmatrix} \begin{bmatrix} f_o' \\ f_r \end{bmatrix} + v(k+1)$$

A Kalman filter based on 5.2.9 was developed to track the random component of the center frequency. Typical results from this filter are shown in Figure 5.2.1 where the sample time is 10 seconds and f_r is generated as shown in Figure 4.3.2. The f_r tracker converges quickly and produces excellent estimates of f_r until a target maneuver is encountered at 500 seconds and Δf changes value. The change in Δf causes a bias in the estimate of f_r. Though $\hat{f}_r$ closely estimates f_r except for this bias, the information is useless unless $\hat{f}_r$ is zero mean. Luckily, this bias can be eliminated, after the target maneuver is complete, by reinitializing the filter. This allows $\hat{f}_o'$ to assume the new Δf as its mean value and $\hat{f}_r$ to return to its desired zero mean. This characteristic of the f_r tracker will be referred to in the next section during a discussion of target maneuvers.

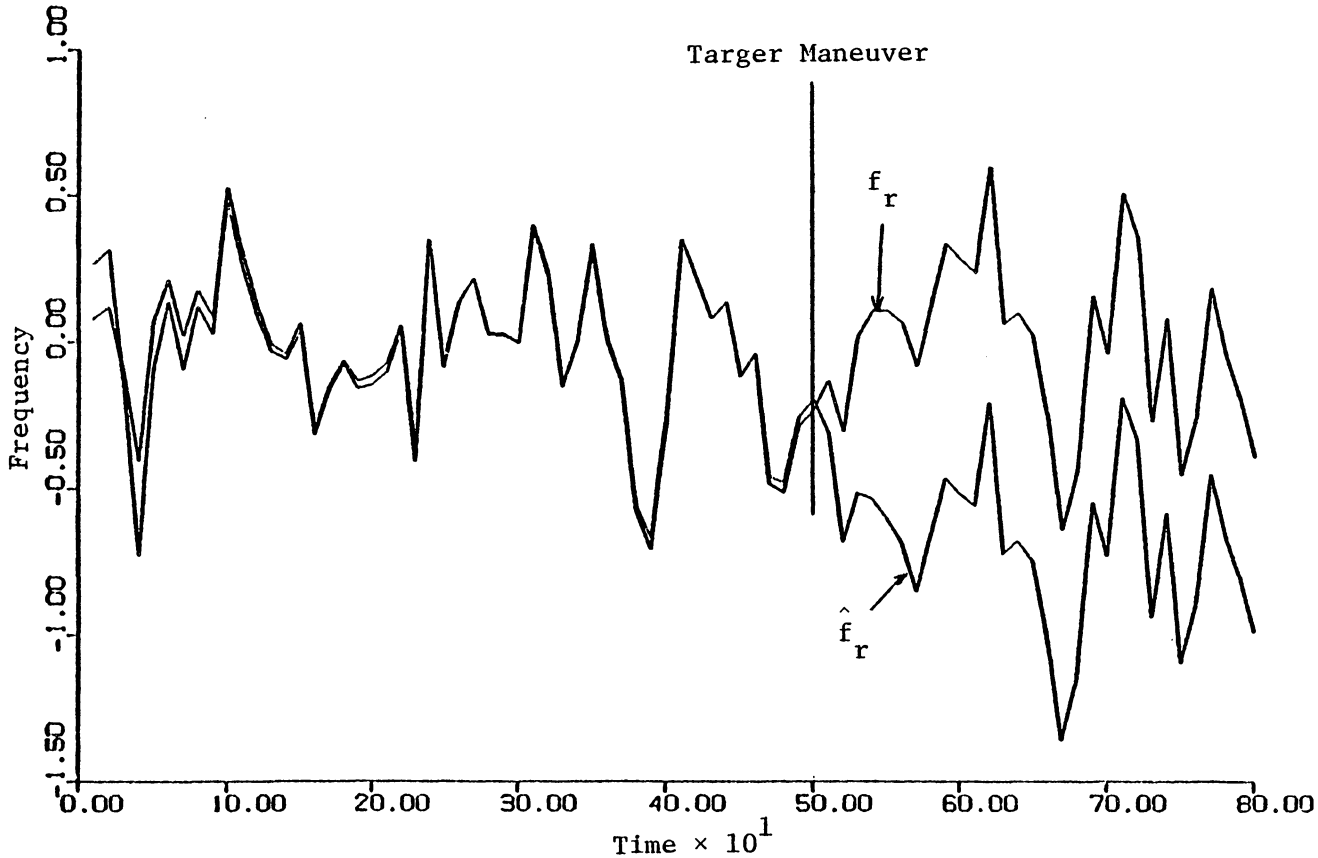

Figure 5.2.1. Random Center Frequency vs. Random Center Frequency Estimate.

5.3 Performance of the Velocity Tracker with Random Center Frequency

With a method for tracking f_r at hand, a velocity tracker based on that discussed in Chapter 4 can be developed to track $\dot{\rho}$ in spite of a random center frequency. A block diagram of the velocity tracker is shown in Figure 5.3.1. This figure shows that $\hat{f}_r$ is simply subtracted from z_f'' to yield an equivalent CCF measurement which is filtered by the velocity tracker of Chapter 4. Before examining the complete adaptive velocity tracker, a single Kalman filter matched to the plant is used to determine the effects of f_r errors on the velocity estimate. The results are shown in Figure 5.3.2 where U_s is .2 and T is 10 sec. This is the same scenario used in Figure 4.3.1. A comparison of these two figures shows that errors in $\hat{f}_r$ do increase the inaccuracy of the final velocity estimate, but not significantly. Once the filter converges, the $\dot{\rho}$ estimates are quite good and show that extension to an adaptive scheme is quite feasible.

The final adaptive filter is achieved by feeding the measurements, $z_f'' - \hat{f}_r$, into the adaptive filter of Chapter 4. Typical results from this velocity tracker with RCF are shown in Figure 5.3.3. The scenario used to generate Figure 5.3.3 is exactly that used for Figure 4.3.3. Comparison of these two figures shows that the velocity tracker with a RCF tracks about as well as does the tracker with CCF.

A final plot 5.3.4 is included to show the effect of measurement noise. This figure compares the random center frequency with the measurement z_f'.

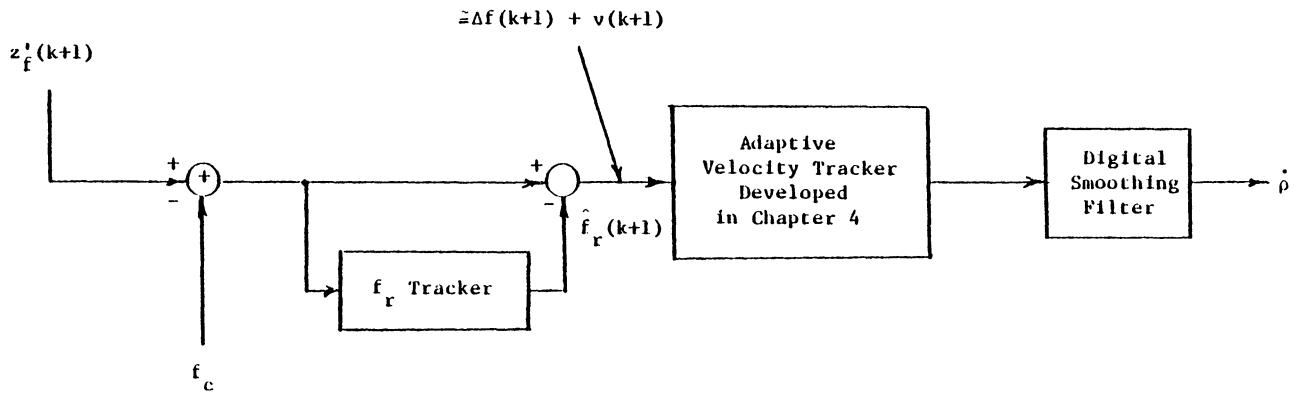

Figure 5.3.1. Block Diagram of Velocity Tracker with Random Center Frequency Scenario.

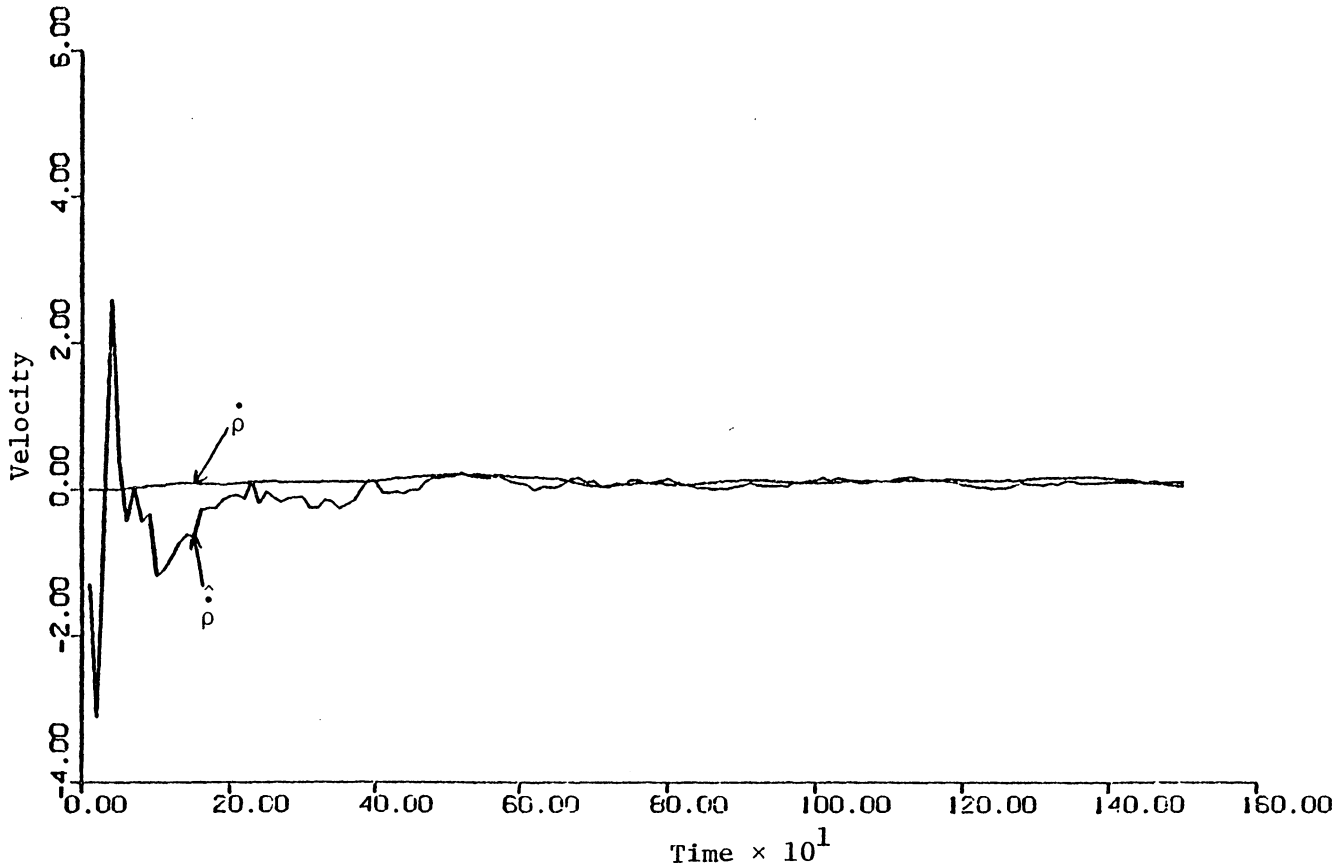

Figure 5.3.2. Velocity vs. Velocity Estimate of a Matched Kalman Filter Using a Random Center Frequency Scenario.

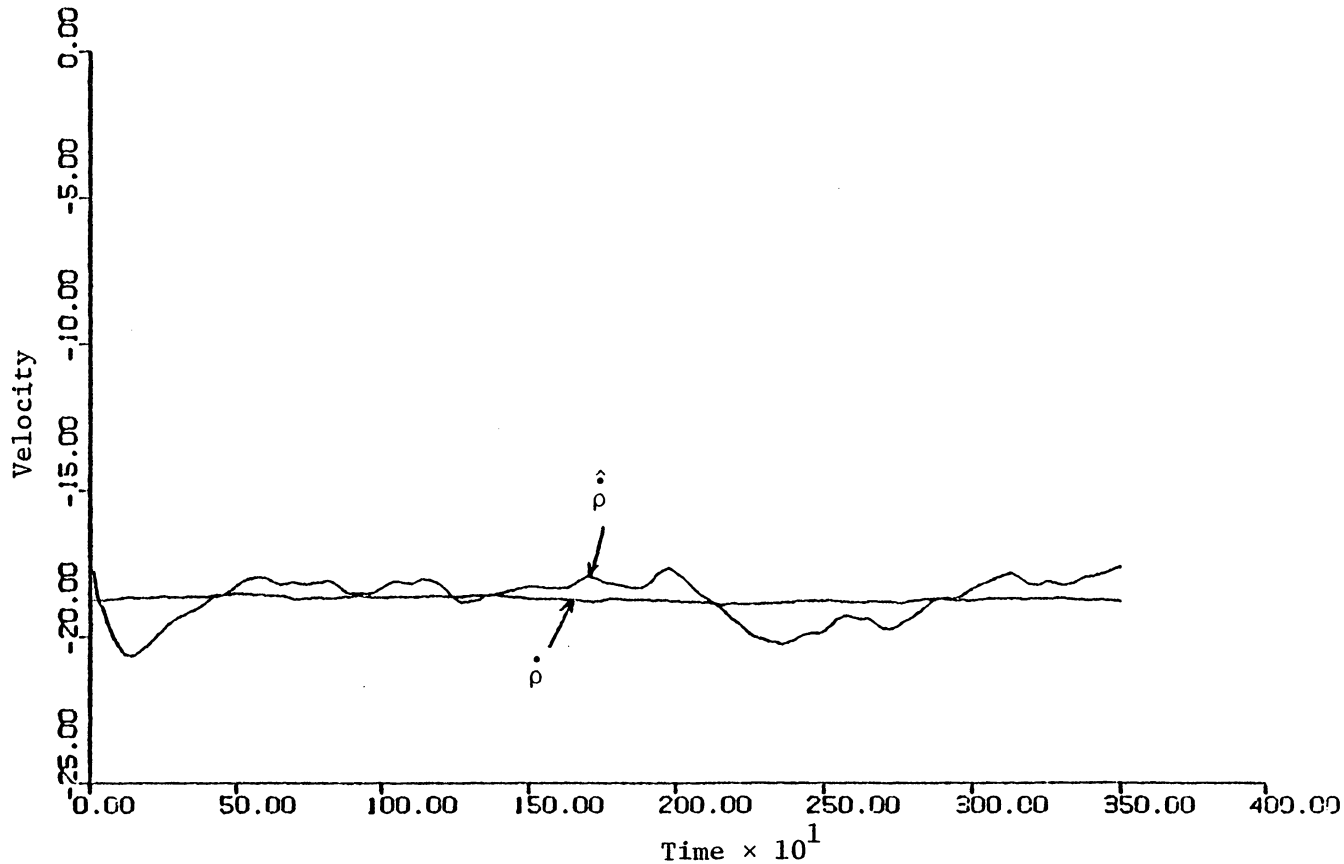

Figure 5.3.3. Velocity vs. Velocity Estimate of an Adaptive Kalman Filter Using a Random Center Frequency Scenario.

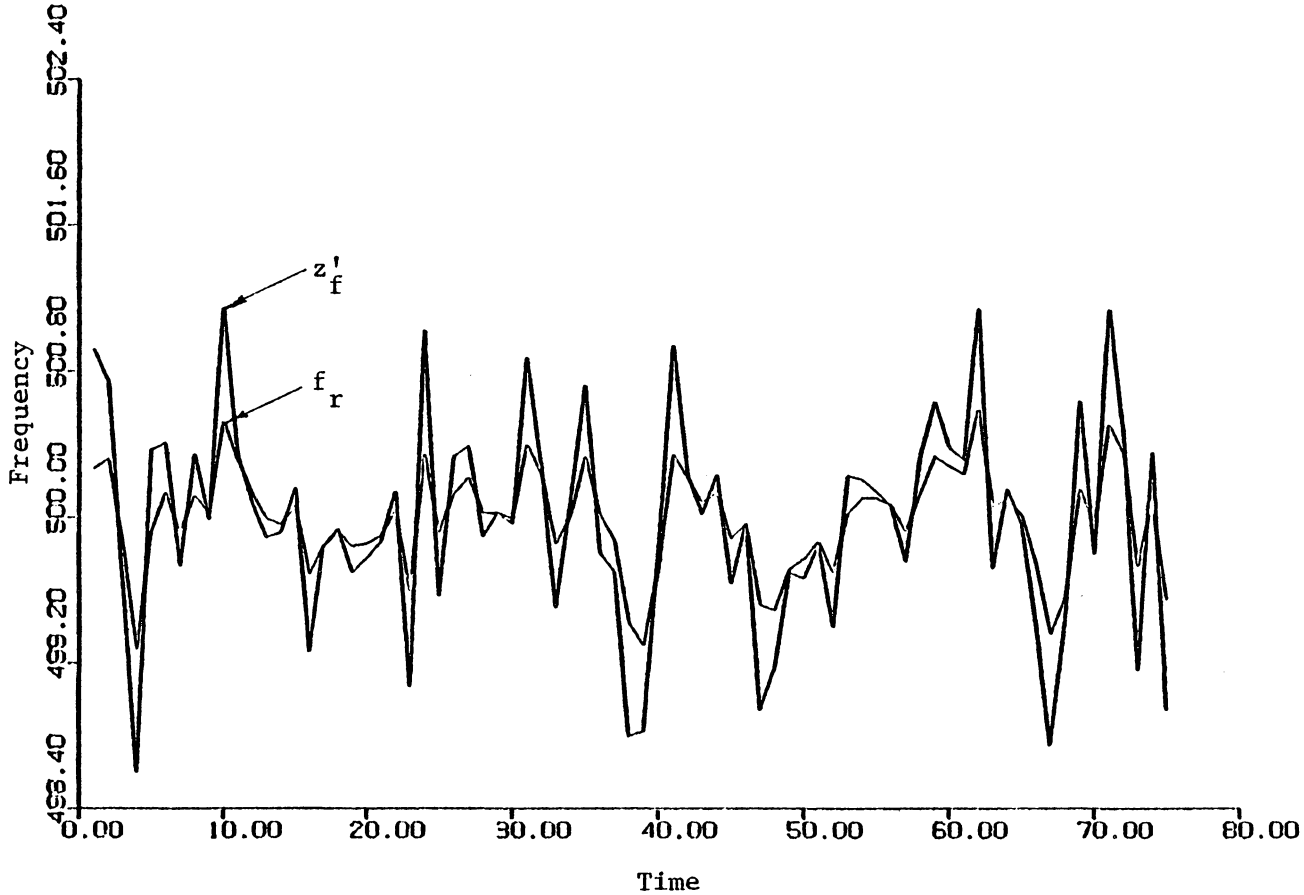

Figure 5.3.4. Illustration of Measurement Noise.

To this point, maneuvers have been neglected so that they could be discussed in light of the tracker just developed. In both the CCF and RCF cases, the Kalman filter gains are allowed to decrease to their minimum values to obtain the most accurate estimates. This procedure works well as long as the target maintains a constant velocity profile. However when a maneuver is encountered, the small gain values combined with a sluggish response by the adaptive weighting factors causes a painfully slow convergence of $\hat{\dot{\rho}}$ to the new value of $\dot{\rho}$.

In the CCF case the convergence can be greatly improved by simply reinitializing the entire tracker once the maneuver is complete. This temporarily increases the gains allowing the Kalman filter to quickly converge to the proper value. The RCF case is further complicated by the bias created in $\hat{f}_r$ during a maneuver. A carefully selected sequence of:

1. waiting for the maneuver to end
2. reinitializing the f_r tracker and waiting for it to converge
3. and reinitializing the adaptive velocity tracker

must be followed to successfully track a maneuver.

The problem of efficiently handling maneuvers with the velocity tracker just developed would merit a chapter of its own if discussed fully. However, discussion of maneuvers shall stop at this point for it is not the intention of this thesis to exhaustively examine this area, but rather to merely expose it as an interesting area requiring further study.

5.4 Conclusion

In real life situations, the center frequency generated by a source is comprised of random and deterministic components. To track the velocity of a source with such a center frequency, an estimate of the random portion must be obtained. A state variable model and an associated Kalman filter have been developed to track f_r which is then subtracted from the current measurement value. The result is filtered by the adaptive Kalman filter of Chapter 4 to produce an estimate of the source velocity. The tracker performance of the RCF case is quite reasonable and is very close to that of the CCF case as long as the target maintains a constant velocity profile. Once a maneuver is encountered, both cases require reinitialization. However, the exact approach needed for the RCF case requires further study.

6. CONCLUDING REMARKS

In this thesis, two adaptive trackers have been developed to estimate the range and/or velocity of maneuvering underwater targets. The trackers process different types of passive measurements so that they can back up and/or complement each other. Both trackers are based on the same basic state equations which model target dynamics in the radial direction. Adaptive tracking techniques allow the trackers to produce reasonable estimates of range and velocity with little or no apriori knowledge.

The range tracker, discussed in Chapters 2 and 3, utilizes a nonlinear prefilter to linearize its time-delay range measurements. This prefilter necessitates the use of several input compensation schemes to make the measurement noise v_ρ suitable for Kalman filtering. The range tracker, though noticeably affected by the input preprocessing, produces excellent range estimates which converge quickly and maintain track even through an abrupt target maneuver. The range tracker is also quite robust, that is, it resists divergence under adverse conditions such as low SNR or an abrupt target maneuver. This is particularly satisfying, for this tracker was developed primarily to avoid the divergence problems inherent to EKF's. The range tracker's velocity estimate could stand improvement, but it is acceptable in light of the estimator's primary range tracking role.

The velocity tracker, discussed in Chapters 4 and 5, processes frequency measurements to provide a second source of velocity estimates. A special Kalman filter has been developed to estimate the

random fluctuations in the target's center frequency. This f_r tracker simplifies the RCF tracking problem to one of CCF tracking which can be handled by an adaptive filter similar to that used by the range tracker. The adaptive velocity tracker provides promising results, but there are a few problems which require further study. Primarily, the trackers sluggish response to target maneuvers.

Our primary goal of demonstrating the validity of the selected adaptive approach has been achieved. The results presented herein show that adaptive tracking techniques are a viable solution to several passive tracking problems. But, this work is intended only as a beginning. Both tracking systems need to be rigorously tested using real data. These tests should include a "fine tuning" process whereby the optimum value for parameters, such as sampling time and filter separation, can be selected. A reinitialization scheme needs to be developed for the velocity tracker which will allow it to quickly converge to the proper velocity after a target maneuver. Once these trackers are in their final form, the area of combined operation must be explored. By sharing results, the individual estimates of these trackers may be improved.

In any case, the results presented demonstrate the potential of the selected tracking schemes. It is hoped that they will also inspire others to extend the ideas developed herein.

REFERENCES

[1] N. H. Gholson and R. L. Moose, "Maneuvering target tracking using adaptive state estimation," IEEE Trans. Aerosp. Electron. Syst., May 1977.

[2] R. L. Moose, "Adaptive target tracking of underwater maneuvering targets using passive measurements," 1981 Annual Report.

[3] R. A. Singer, "Estimating optimal tracking filter performance for manned maneuvering targets," IEEE Trans. Aerosp. Electron. Syst., July 1970.

[4] R. L. Moose, "Adaptive estimator for passive range and depth determination of a maneuvering target (U)," U. S. Naval J. Underwater Acoustics, July 1973.

[5] R. A. Howard, "System analysis of semi-Markov processes," IEEE Trans. Mil Electron., vol. MIL-8, pp. 114-124, April 1964.

[6] A. H. Jazwinski, "Limited memory optimal filtering," IEEE Trans. Automat. Contr., vol. AC-13, Oct. 1968.

[7] J. S. Thorp, "Optimal tracking of maneuvering targets," IEEE Trans. Aerosp. Electron. Syst., vol. AES-9, July 1973.

[8] J. C. Hassab, "Passive tracking of a moving source by a single observer in shallow water," Journal of Sound and Vibration (1976) 44 (1).

[9] D. H. McCabe, "Adaptive estimation techniques for tracking airborne and underwater maneuvering targets," Ph.D. dissertation at VPI&SU, May 1979.

APPENDIX A

The basic Kalman filter equations used in this thesis are described below.

Given a state variable model of the form

$$\underline{X}(k+1) = \phi\, \underline{X}(k) + \Gamma\, \underline{U}(k) + \psi\, w(k)$$

where

$\underline{X}$ is a vector containing the state variables

ϕ is the state transition matrix

$\underline{U}$ is a deterministic input vector related to the sources velocity

Γ is a transition matrix associated with U

ψ is the input transition matrix

w is a Gaussian zero-mean white noise process

k is the discrete time parameter

and the measurement equation

$$z(k+1) = H\, \underline{X}(k) + V(k+1)$$

where

z is the measurement

H is a vector describing the relationship between the measurement and the state variables

V is a zero-mean Gaussian noise process

the Kalman equations are:

1. The estimate equation

$$\hat{\underline{X}}(k+1) = \phi\hat{\underline{X}}(k) + \Gamma\underline{U}(k) + G(k+1)[z(k+1) - H(\phi\hat{\underline{X}}(k) + \Gamma\underline{U}(k))]$$

2. The gain equations

$$G(k+1) = M(k+1)H^T(HM(k+1)H^T + R)^{-1}$$

$$M(k+1) = \phi P(k)\phi^T + \psi Q\psi^T$$

$$P(k+1) = (I - G(k+1)H)M(k+1)$$

where

$\hat{\underline{X}}$ is the estimate of the state variables

G is the filter gain

$P(k) = E[(\underline{X} - \hat{\underline{X}})(\underline{X} - \hat{\underline{X}})]_K$

$Q = E[w \cdot w^T]$

I is the identity matrix

Note: The range tracking Kalman filters require a third term in the equation for M(k+1). This term is

$$\Gamma \frac{\Delta U^2}{12} \Gamma$$

where

ΔU is the difference between two consecutive $U_s^{(i)}$'s in the adaptive filter bank.

The reason for this term and its derivation are given in Reference 2.

The vita has been removed from the scanned document

EXAMINATION OF SELECTED PASSIVE TRACKING SCHEMES USING ADAPTIVE KALMAN FILTERING

by

Timothy E. Dailey

(ABSTRACT)

In the past, passive SONAR range tracking systems have used Extended Kalman filters to process nonlinear time-delay measurements. This approach has several flaws due to the inherent divergence problems of Extended Kalman filters. This paper discusses a new approach which uses a prefilter to linearize the measurements so that they can be processed by a standard Kalman filter. The approach is subsequently expanded for use with an adaptive Kalman filter which allows source maneuvers to be tracked.

A new approach to passive Doppler velocity tracking is also proposed which uses a dedicated Kalman filter to track random fluctuations in the sources center frequency. This dedicated tracker simplifies the problem so that it can be handled by a basic adaptive Kalman filter.